Structure and Evolution of a Cumulonimbus Cloud Developed over a Mountain Slope with the Arrival of Sea Breeze in Summer

Tetsuya SANO and Kazuhisa TSUBOKI

Hydrospheric Atmospheric Research Center, Nagoya University, Nagoya, Japan

Abstract

Cumulonimbus clouds frequently develop over mountains, a plain, and the sea in the summer in association with thermally induced local circulations. On July 5, 2000, when the sea breeze from the Pacific Ocean blew over the Noubi Plain and arrived at the slope of the Ibuki Mountains where a valley wind circulation developed, a cumulonimbus cloud occurred over the slope of the Ibuki Mountains. In this paper, the structure and evolution of the cumulonimbus cloud are investigated using the data of Doppler radars.

The direction of the environmental vertical wind shear was southeast, which is parallel to the slope of the Ibuki Mountains, when the cumulonimbus cloud occurred. The cumulonimbus cloud maintained for about 2 hours. The cumulonimbus cloud consisted of groups of precipitating cells; "Primary Cell" and "Secondary Cells." The former developed with tilting toward the downshear side and moved down the slope. The latter developed almost uprightly on the upshear side of the Primary cell. There were 6 groups of cells in the cumulonimbus cloud.

The developing process and structure of group C, which was the most intense group, were investigated in detail. After Primary Cell C1, with tilting toward the downshear side, developed, Secondary Cells C2, C3 and C4 of group C developed on the upshear side (the Ibuki Mountains side) of cell C1. An outflow from cell C1 toward the upshear side of cell C1 lifted the low-level air. Cells C2, C3 and C4 developed almost uprightly on the upshear side of cell C1, where the convection of cell C1 weakened the vertical wind shear. Cells C3 and C4 had maximum reflectivety of over 50 dBZ and the echo top of 15 km above sea level (ASL). Cells C3 and C4 developed explosively in the group C due to the horizontal convergence at the middle layer, which was strengthened by the outflow from cell C2, the northeasterly inflow toward cells C3 and C4, and the lifted low-level air on the Ibuki Mountains side.

1. Introduction

In summer, cumulonimbus clouds frequently develop over mountains, a plain and the sea where thermally induced local circulations develop; a valley wind circulation and a sea breeze circulation. Such cumulonimbus clouds occasionally cause localized heavy rainfall. They are one of the dominant elements in the

Corresponding author: Tetsuya Sano, Hydrospheric Atmospheric Research Center, Nagoya University, Nagoya 464-8601, Japan.
E-mail: sano@rain.hyarc.nagoya-u.ac.jp

water circulation process associated with thermally induced local circulations.

A valley wind circulation develops over a mountain slope in the daytime. It transports heat to the valley and water vapor to the mountain (Kimura and Kuwagata 1995; Kuwagata and Kimura 1997). The transportation of heat was observed by a sounding in the Ina Valley (Kuwagata and Kimura 1995) and by the analysis of routine meteorological data in central Japan (Kuwagata et al. 1990). The transportation of water vapor to the mountain was observed by a sounding over the Northern Mountains on the Kanto Plain (Kimura et al. 1997). Kimura (1994) indicated that the sunshine du-

ration over mountains decreased in the afternoon on calm days, reflecting the transportation of water vapor to mountains associated with the valley wind circulation. Kuwagata (1997) showed a decrease in sunshine duration over mountains, and pointed out that the accumulated moist air over mountains contributes to the formation of cumulus clouds. Moreover, the transportation of water vapor to the mountain in the daytime resulted in the diurnal variation of precipitable water. This was revealed by an analysis of Global Positioning System (GPS) data (Sasaki and Kimura 2001; Iwasaki and Miki 2001).

The relationship between the occurrence of cumulonimbus clouds and convective precipitation over mountains and the valley wind circulation has been found by statistical studies. The frequency of convective precipitation increases over mountains and islands in the afternoon and evening (Fujibe 1988; Kuwagata 1997; Saitoh and Kimura 1998). Kuwagata (1997), and Saitoh and Kimura (1998) pointed out that the increment in the frequency of convective precipitation in the afternoon is related to the transportation of water vapor by the valley wind circulation. Iwasaki and Ohbayashi (1998) showed that many cumulonimbus clouds with hail occur over the mountainous and semi-basin areas of Gunma Prefecture in the afternoon and evening. The occurrence of cumulonimbus clouds corresponds to the time when the valley wind circulation develops.

Convective precipitation over a mountain slope is related to the structure and developing process of a cumulonimbus cloud that developed over such a slope. Caracena et al. (1979) studied the Big Thompson storm, which was severe and caused heavy rainfall over the Big Thompson Canyon, Colorado, U.S., and found that the storm was caused by an upslope orographic lifting and remained as a result of a stationary inflow of moisture at the lower layer. Yoshizaki and Ogura (1988) showed in two- and three-dimensional numerical simulations of the Big Thompson Storm that convective cells continually developed at the foot of the slope and organized toward the upslope side. Cotton et al. (1983) studied a mesoscale convective complex developed over South Park, U.S., and found that cumulonimbus clouds occurred around the top of the slope in South Park and organized toward the downslope side. Tripoli and Cotton (1989) explained the mechanism of organization toward the downslope side of cumulonimbus clouds with the use of a two-dimensional numerical model. In their cases, however, the phenomena occurred when synoptic disturbances of a low and a front were present in the lower layer. The structure and evolution of the cumulonimbus clouds that developed over the mountain slope where the valley wind circulation developed have not been described in detail. The contribution of the valley wind circulation to the structure and evolution of cumulonimbus clouds that develop over the slope of the mountain is not sufficiently understood.

A sea breeze circulation that develops between the sea and a plain is another important thermally induced local circulation. A sea breeze usually forms a convergence of low-level wind at the leading edge, which is referred to as a sea breeze front (Atkinson 1981). Cumulonimbus clouds occurred at the convergent region in association with a sea breeze front over Florida (e.g., Nicholls et al. 1991; Pielke 1991). Pielke (1974) showed, in a three-dimensional numerical simulation, that the location of thunderstorms along the east coast of Florida was controlled by the location and movement of the sea breeze.

Wilson and Megenhardt (1997), however, indicated that cumulonimbus clouds associated with a sea breeze alone along the east coast of Florida were small and short-lived, because the convergence of the sea breeze was weak. The collisions and interactions of a sea breeze and the outflow of a pre-existing thunderstorm caused cumulonimbus clouds (Simpson et al. 1980; Kingsmill 1995; Wilson and Megenhardt 1997). Wakimoto and Atkins (1994) and Atkins and Wakimoto (1995) discovered through their observations in Florida that clouds developed in areas where the updraft of horizontal convective rolls merged with the updraft developed by a sea breeze front. Dailey and Fovell (1999) explained, using a numerical simulation, that convections are enhanced in the areas where updrafts are strengthened by the interaction of a sea breeze and horizontal convective rolls.

Over complex terrain including mountains, a plain, and the sea, thermally induced local circulations coexist and are complicated. Kurita et al. (1988) indicated that the complex struc-

ture of the wind distribution consisted of a valley wind and a sea breeze in the Kanto District. Kondo (1990a, 1990b) discussed the interaction of a valley wind and a sea breeze. Iwasaki (2004) studied precipitable water and convective activity in the summer season at Mt. Tanigawa, which exhibited a diurnal variation. It found that the maxima of precipitable water in the daytime were caused by the moisture transport associated with a valley wind circulation from early morning to noon and those in the evening were caused by the moisture convergence from the "extended sea breeze" according to Kondo (1990a) from around 15 Japan Standard Time (JST) to late at night. These maxima of precipitable water coincided with the maxima of convective activity. However, the structure and evolution of a cumulonimbus cloud which occurred over the complex terrain with the thermally induced local circulations are not thoroughly understood.

The Noubi Plain is surrounded by the mountainous region to the north and the sea to the south (Fig. 1); it is one of the regions where thermally induced local circulations develop over the complex terrain in summer (Owada 1994). Mori et al. (1994) indicated that the "sea breeze" from the Pacific Ocean dominated over the Noubi Plain in the afternoon after the development of the "small-scale sea breeze" from Ise Bay in the morning. When the thermally induced local circulations develop without significant synoptic disturbances on the surface in summer, cumulonimbus clouds frequently occur over the surrounding mountains and the Noubi Plain.

From June to September 2000, we carried out Doppler radar observations to examine the precipitation in the Noubi Plain and around the mountainous region. During the Doppler radar observation, cumulonimbus clouds which developed over the regions with a valley wind and a sea breeze were observed. In the present study, we examine the structure and evolution of a cumulonimbus cloud that had developed over a mountain slope where a valley wind circulation developed and a sea breeze arrived. The main focus was on the structure, movement, and development of the cellular echoes in the cumulonimbus cloud. The objectives of this study are to elucidate the structure of cumulonimbus cloud that caused heavy rainfall
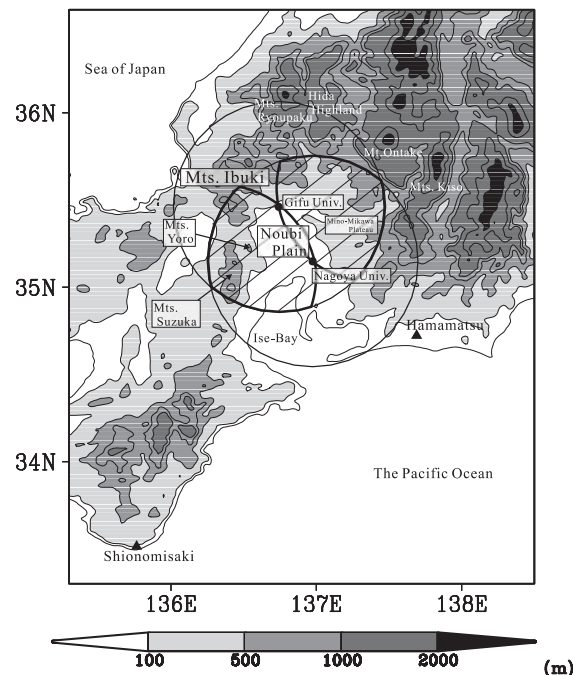

Fig. 1. Map of the observation area. The two closed circles indicate the sites of the Doppler radars (Nagoya University and Gifu University). Each circle indicates the observation range of each Doppler radar. The hatched areas are the dual Doppler radar processing regions. The closed triangles indicate the upper-air sounding stations (Shionomisaki and Hamamatsu). The contours of the topography are 100, 500, 800, 1000, 1500, and 2000 m ASL.

over a mountain region, and to understand the roles of a valley wind circulation and a sea breeze in the development of a cumulonimbus cloud.

2. Observation and data

The Noubi Plain is surrounded by the Ibuki Mountains, the Ryopaku Mountains and the Hida Highland to the north, Mt. Ontake and the Kiso Mountains to the east where have the Mino-Mikawa Plateau at the foot of them, and the Suzuka Mountains and the Yoro Mountains to the west (Fig. 1). From June to September 2000, two X-band Doppler radars of Nagoya University were located at Nagoya University and Gifu University, to observe precipitating clouds in summer in the Noubi Plain and its

surroundings.

The maximum range of observation for each Doppler radar is 64 km. Each Doppler radar performed Plain Position Indicator (PPI) volume scans with a time interval of 7 minutes. The PPI scans of the Nagoya University radar were stepped up from 0.5 to 33.6 degrees with 13 elevation angles, and those of the Gifu University radar were stepped up from 0.6 to 40.9 degrees with 14 elevation angles. The Cressman filter (Cressman 1959) was used to interpolate the radial Doppler velocity and reflectivity in the Cartesian coordinate. The horizontal and vertical grid intervals were 500 m. To draw the three-dimensional distributions of the Doppler velocity and reflectivity, a correction related to the movement of the radar echo was made using Gal-Chen's method (Gal-Chen 1982). For the correction related to the movement, the speed of the convective echo was used. The central time of the correction related to the movement of the radar echo was 3 minutes after each volume scan started. The horizontal velocity was derived at grid points from the dual Doppler radar observation data. The observations made with the Gifu University radar had a shadowed area on the north and northeast because of obstructions near Gifu University. Therefore, the vertical motion is infered from the horizontal divergence derived from the horizontal velocity because the vertical velocity was not accurately derived from the upward integration of the continuity equation with the boundary condition of 0 m s^{-1} at the surface.

In addition to the Doppler radar data, conventional radar data of the Japan Meteorological Agency (JMA), the Automated Meteorological Data Acquisition System (AMeDAS), Geostationary Meteorological Satellite (GMS) infrared images, upper-air sounding data at Hamamatsu and Shionomisaki, and synoptic weather maps of the JMA publication were used for this study. Local Standard Time (LST = UTC + 9 hours) is used in the present paper.

3. Occurrence distribution of cumulonimbus clouds and features of thermal induced local circulations

Cumulonimbus clouds frequently occur in the summer when a synoptic disturbance is in-

significant in the lower layer. The occurrence distribution of cumulonimbus clouds over the Noubi Plain and the surrounding mountains was investigated with the use of the JMA radar. The period of the analysis was July and August 2000. We selected the 20 days when cumulonimbus clouds occurred without significant synoptic disturbances over the Noubi Plain using a surface weather map at 0900 LST.

In this section, fully developed cumulonimbus clouds are defined by the JMA radar echoes with rainfall intensity over 32 mm h^{-1}. The points at which the mature cumulonimbus clouds occurred are defined by the point at which the rainfall intensity of the echoes that reaches 16 mm h^{-1} first using a backward trace. The time of the analysis was from 1200 LST to 1900 LST. The area of the analysis was between 34.5°N and 36.3°N, and 136.1°E and 138°E, including the Noubi Plain.
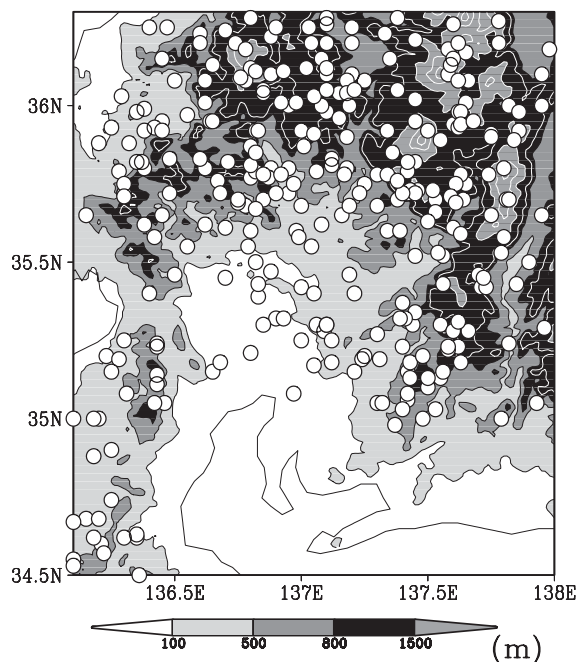

Fig. 2. Distribution of occurrence points of cumulonimbus clouds. The white dots are occurrence points of cumulonimbus clouds. The shaded areas are the topography. The black contours at 100 and 500 m ASL. The white contours at 1000, 1500, 2000 and 2500 m ASL.

Figure 2 shows the occurrence distribution of the cumulonimbus clouds. Most cumulonimbus clouds occurred in regions higher than 500 m above the mean sea level (ASL). In particular, the occurrence points of cumulonimbus clouds concentrated over the slopes and peaks of the Ryopaku Mountains, the Kiso Mountains, Mt. Ontake and the Hida Highland where have peaks of about 1500 m ASL and above. Many cumulonimbus clouds also occurred over the slopes and peaks of the Ibuki Mountains and the Suzuka Mountains where have peaks of about 1000 m ASL.

Figure 3a shows the wind and deviation of temperature from 0900 LST averaged for 20 days at 1000 LST. In the mountains, the increase in the temperature from 0900 LST was large. Valley winds over the slopes of the mountains blow toward peaks where the temperature had increased. In the coastal region of Ise Bay, the increase in the temperature from 0900 LST was smaller than that in the mountains, and the wind originated from Ise Bay. This wind is the "small-scale sea breeze" from Ise Bay. Over the Noubi Plain, a weak and irregular wind blows, which cannot be identified as either a valley wind or a small-scale sea breeze.

Figure 3b is the same as Fig. 3a, but at 1500 LST. Over the slopes of the mountains, the Mino-Mikawa Plateau and the inner Noubi Plain, the increase in the temperature from 0900 LST was larger than that at 1000 LST and valley winds developed. The gradient of the temperature was large, and a southerly wind developed between the inner Noubi Plain and the coast of the Pacific Ocean. The "sea breeze" from the Pacific Ocean developed and intruded into the inner Noubi Plain in the afternoon. Mori et al. (1994) showed that the small-scale sea breeze is replaced by the sea breeze around 1500 LST at Nagoya.

Thus, cumulonimbus clouds developed over the mountainous region surrounding the Noubi Plain when the valley wind over the mountainous region and the sea breeze over the Noubi Plain developed.

4. Case study on July 5, 2000

On July 5, 2000, a cumulonimbus cloud developed over the slope of the Ibuki Mountains when the "sea breeze" arrived at the
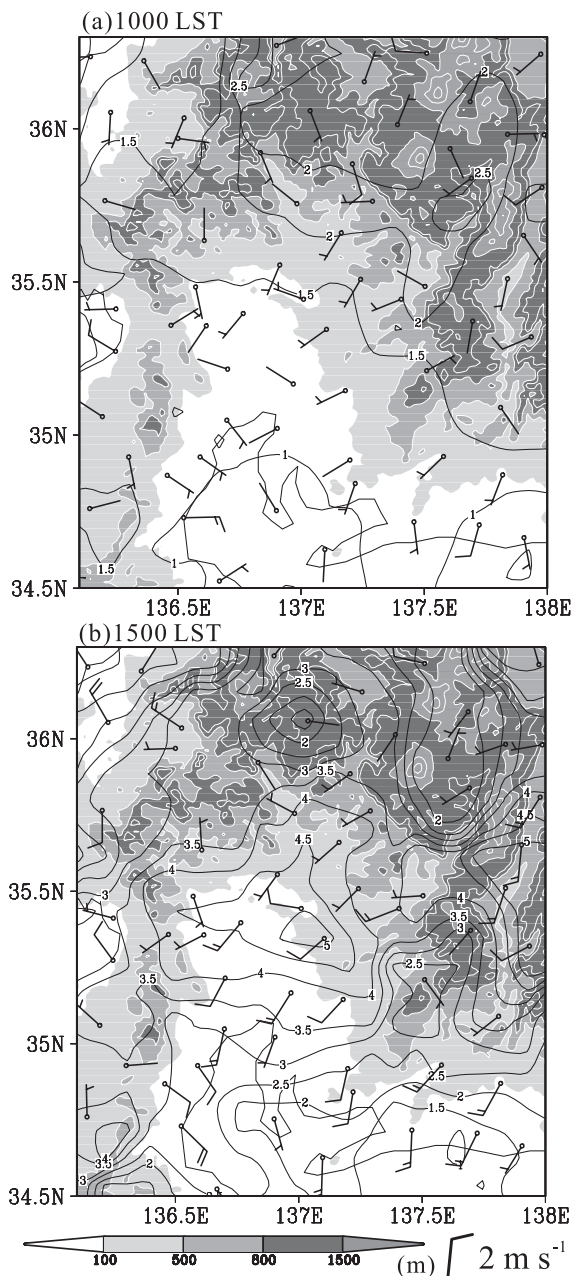

Fig. 3. Wind and deviation of temperature from 0900 LST at (a) 1000 LST and (b) 1500 LST averaged over 20 days. The white contours with shading are the topography at 100, 500, 800, 1000, 1500, 2000 and 2500 m ASL.

slope. In the following sections, the case is described as an example of cumulonimbus clouds over the slope of mountains adjoining the Noubi Plain.
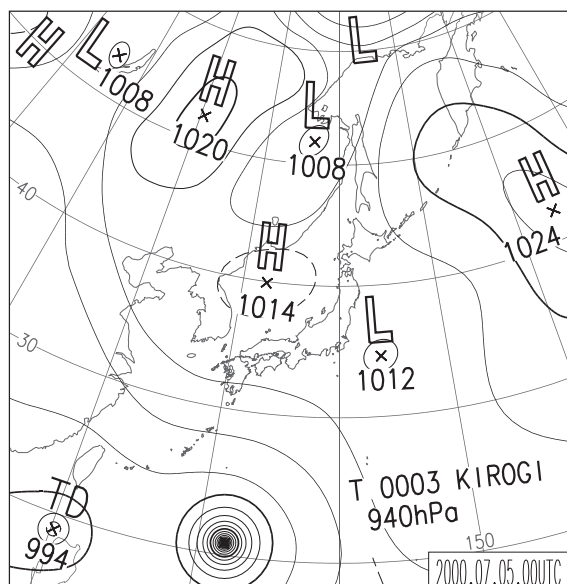
Fig. 4.   Surface synoptic map at 0900 LST July 5, 2000. The source of surface synoptic map is the JMA publication.
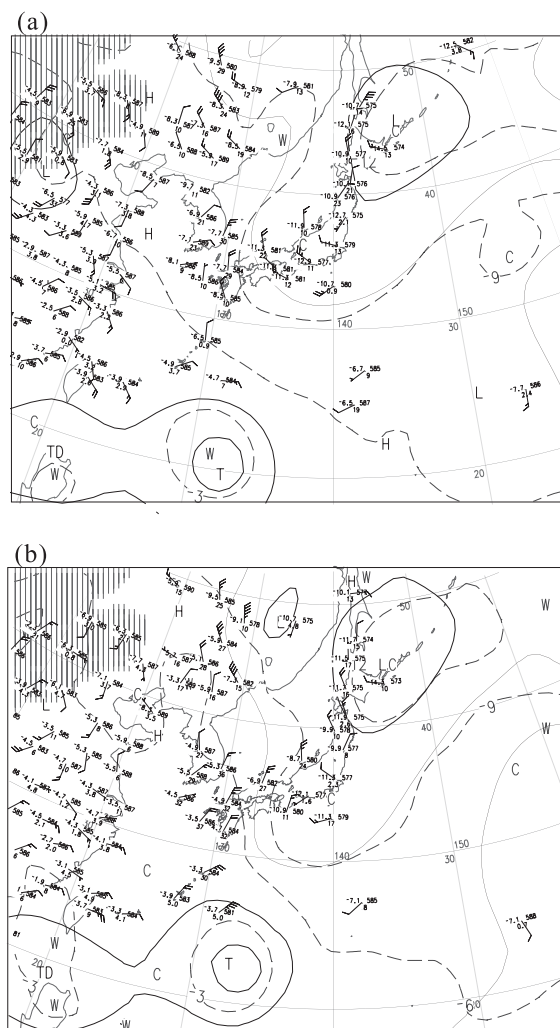

Fig. 5.   Upper-level synoptic maps at 500 hPa at (a) 0900 LST and (b) 2100 LST July 5, 2000. The source of upper-level synoptic maps is the JMA publication.

4.1   Synoptic conditions

Weather maps at 0900 LST July 5, 2000, are shown in Figs. 4 and 5. A high was present in the vicinity of Japan, and a synoptic disturbance was weak on the surface in central Japan, although a weak low was located to the southeast of Japan (Fig. 4). On the other hand, the upper-level weather map at 500 hPa at 0900 LST shows that a trough with cold air of $-9°C$ was present over Japan (Fig. 5a), and moved eastward at 2100 LST (Fig. 5b).

The sounding profile at Hamamatsu at 0900 LST July 5, 2000, is shown in Fig. 6. The convective mixed layer was developing below 850 hPa. The air was almost saturated at about 850 hPa, while a dry layer was present between 850 and 700 hPa. An inversion layer was present around 800 hPa. The layer from 750 to 500 hPa was convectively unstable. The convective available potential energy (CAPE) was about 500 J kg^{-1}. Chuda and Niino (2005) indicated that the monthly median of CAPE at Shionomisaki at 0900 LST in July for 1990~1999 was 1728 J kg^{-1}. The CAPE in this case was small. The lifting condensation level (LCL) was about 1.2 km ASL. The level of free convection (LFC) was about 3 km ASL. Under

this condition, a strong trigger was necessary for the occurrence of cumulonimbus clouds.

The wind hodograph obtained from the Shionomisaki sounding at 1500 LST July 5, 2000, is shown in Fig. 7 although no sounding data were obtained at Hamamatsu in the period of the observation. The SW-ly wind was present at 2 km ASL. The northerly wind was between 3 and 5 km ASL. The NW-ly wind was above 6 km ASL. The magnitude and direction of the vertical wind shear between 2 and 9 km ASL
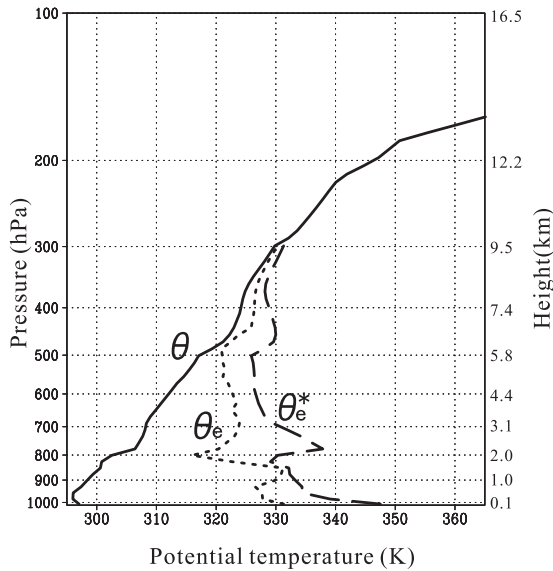
Fig. 6. Upper-air sounding profiles at Hamamatsu at 0900 LST July 5, 2000. The solid, dotted and dashed lines are the potential temperature (θ), equivalent potential temperature (θ_e), and saturated equivalent temperature (θ_e^*), respectively.

Fig. 8. Distribution of GMS infrared images at (a) 1234 LST and (b) 1534 LST. The white areas over land are TBB (°C). The contours in the white areas are drawn under −20°C every −5°C. The thin white contours with shading indicate the topography.
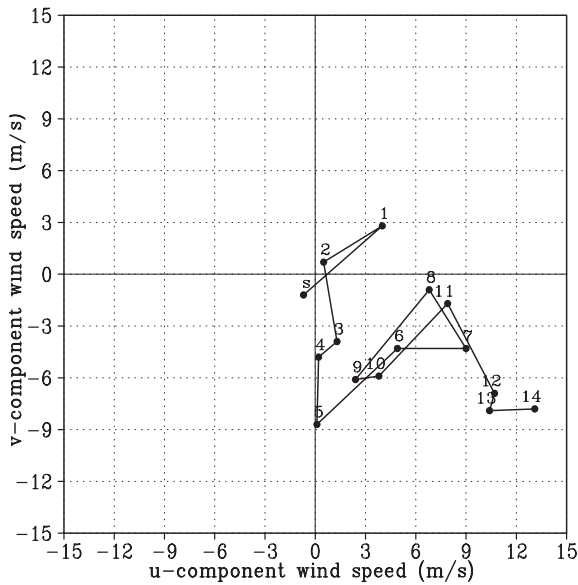

Fig. 7. Hodograph at Shionomisaki at 1500 LST July 5, 2000. The numbers in the figure indicate the altitude (km). S indicates the surface wind.
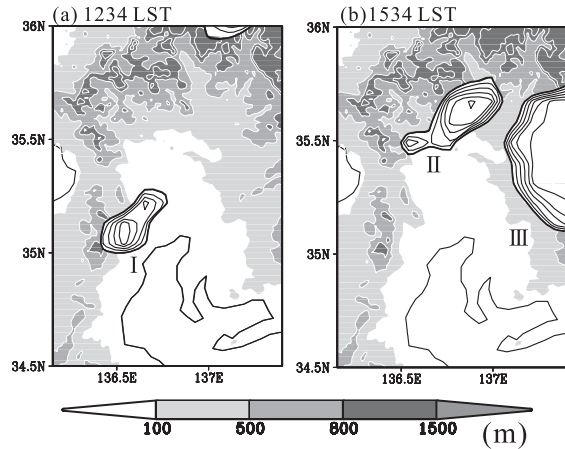
were about 0.8×10^{-3} s^{-1} and 164° in azimuth, respectively. The directions of the vertical wind shears at 0900 LST and at 2100 LST were eastward and southward, respectively, and these magnitudes were bigger than those at 1500 LST (not shown). The direction of the vertical wind shear rotated clockwise from eastward to southward. The variation of the vertical wind shear correlated the eastward movement of the trough with the cold air at 500 hPa (Fig. 5). The cumulonimbus cloud of the study occurred when the cold trough was moving over the Japan Islands.

Figure 8 shows GMS infrared images around the Noubi Plain. Cloud area I, whose minimum TBB was under −40°C, appeared over the slope of the Suzuka Mountains and the Yoro Mountains at 1234 LST (Fig. 8a). Cloud area II (the target cloud in the present study), which had a low TBB, appeared over the slope of the Ibuki Mountains at 1534 LST (Fig. 8b). Under this synoptic condition, tall and developed cumulonimbus clouds appeared over the slope of the mountains adjoining the Noubi Plain. Cloud area III over the Mino-Mikawa Plateau moved from the northeast mountainous area. Cloud area III is not discussed in the present study.
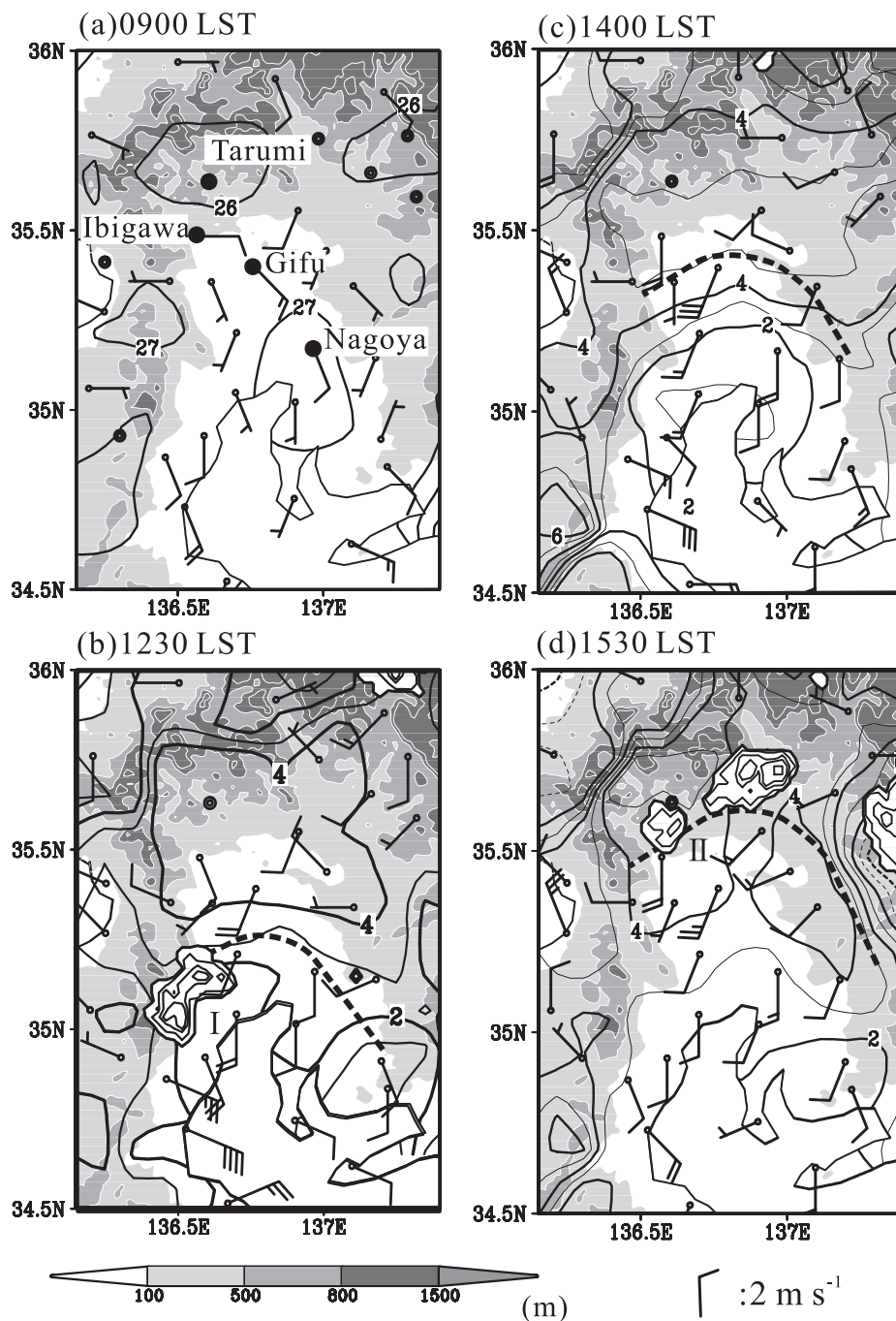
Fig. 9.   (a) Sea level temperature and wind at 0900 JST on July 5, 2000. The black contours are the temperature at the mean sea level with a lapse rate of $6.5°C\ km^{-1}$ and are drawn every $1°C$. The barbs are the wind direction and wind speed at the AMeDAS observation points. The dashed line is the position of the sea breeze front deduced from AMeDAS. The thin white contours indicate the topography. Distribution of the radar echo of the JMA radar and difference of the temperature from 0900 LST and wind at (b) 1230 LST, (c) 1400 LST and (d) 1530 LST on July 5, 2000. The white areas over land are the radar echoes. The contours in the white areas are drawn at 1, 4, 16, 32, and $64\ mm\ h^{-1}$. The black contour lines are the difference of the temperature from 0900 LST and are drawn every $1°C$.

4.2 Surface conditions over the Ibuki Mountains and the Noubi Plain

Figure 9a shows the sea level temperature calculated with a lapse rate of 6.5°C km^{-1}, and wind at AMeDAS observation points at 0900 LST July 5, 2000. Figures 9b–9d show the radar echoes of the JMA, the deviation of the temperature from 0900 LST, and the wind at (b) 1230 LST, (c) 1400 LST, and (d) 1530 LST. The dashed thick line in Figs. 9b–9d indicates the front associated with the sea breeze from the Pacific Ocean, which is named the "sea breeze front." We determined the position of the sea breeze front by the development of the southerly component of wind with the decrease or dull increase of the temperature at each AMeDAS point.

At 0900 LST (Fig. 9a), winds toward the peaks of the mountains were observed at the AMeDAS points over the slopes. This indicates that a valley wind began to blow. At 1230 LST (Fig. 9b), the increase in the temperature from 0900 LST was large in the inner plain and at the slopes of the mountains, and a valley wind developed. This condition continued until 1400 LST (Fig. 9c).

Figures 10a–10d show the time variations of the temperature, wind and sunshine duration observed by AMeDAS at Tarumi on the Ibuki Mountains, Ibigawa at the foot of the Ibuki Mountains, Gifu in the inner Noubi Plain, and Nagoya in the coastal area of the Noubi Plain.

At Tarumi (Fig. 10a), the sunshine duration remained at 8∼10 minutes / 10 minutes and the temperature increased until 1300 LST. The sunshine duration became zero from 1310 LST, due to clouds over the Ibuki Mountains. The temperature remained at 28∼29°C from 1310 LST. No wind was observed until 1530 LST. At Ibigawa (Fig. 10b), long sunshine duration was observed from the morning until 1450 LST. Temperature started to increase from the morning. The temperature began to increase abruptly at 1330 LST and remained at about 32°C until 1450 LST. A weak SSE-ly wind developed from 1000 LST. The wind gradually became strong after 1200 LST and changed into a southerly wind at 1340 LST. The southerly wind was the valley wind that had developed over the Ibuki Mountains. These conditions are the result of the heat transportation toward the foot and the water vapor transportation to-
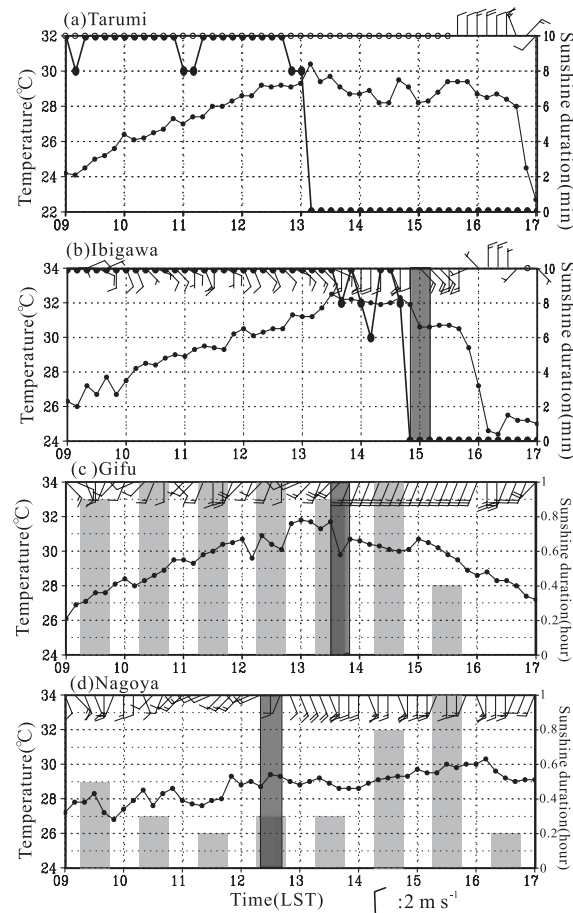

Fig. 10. Time variation of AMeDAS data at (a) Tarumi, (b) Ibigawa, (c) Gifu, and (d) Nagoya between 0900 LST and 1700 LST July 5, 2000. The locations of the AMeDAS points are shown in Fig. 9a. The thick line in (a) and (b) is the sunshine duration every 10 minutes. The bar in (c) and (d) is the sunshine duration every 1 hour. The barbs represent the wind. The solid line with dots is the temperature in (b), (c) and (d). The barbs indicate the direction and speed of wind. The gray shaded areas are the periods of the passage of the sea breeze front.

ward the peak, associated with the valley wind circulation developed over the slope of the Ibuki Mountains.

At 0900 LST (Fig. 9a), weak winds with a southerly component blew over the Noubi Plain. In the coastal region, a small-scale sea breeze blew. At Nagoya (Fig. 10d), a weak undecided

wind with short sunshine duration blew until 1030 LST. On the other hand, a weak undecided wind with long sunshine duration blew until 1130 LST at Gifu (Fig. 10c). This wind was generated by the effect of the local cloud cover. The SW-ly and SSW-ly wind blew between 1040 LST and 1220 LST with short sunshine duration at Nagoya (Fig. 10d). This wind was the small-scale sea breeze from Ise Bay.

At 1230 LST (Fig. 9b), the increase in the temperature from 0900 LST in the coastal region was smaller than that in the inner plain and the slopes, and southerly and SSE-ly winds developed. The gradient of the temperature over the Noubi Plain intensified. Radar echo I appeared between the Suzuka and the Yoro Mountains. Radar echo I corresponds to cloud area I (Fig. 8a). At Nagoya (Fig. 10d), the time variation in the temperature became small from 1230 LST, although the long sunshine duration continued between 1400 and 1600 LST and southerly, or SSE-ly, winds developed after 1230 LST. The sea breeze from the Pacific Ocean arrived and developed at Nagoya. The cumulonimbus cloud occurred when the sea breeze front arrived at the foot of the Suzuka and the Yoro Mountains (Fig. 9b).

The temperature in the Noubi Plain at 1400 LST was almost unchanged from 1220 LST, and a southerly wind prevailed (Fig. 9c). At Gifu (Fig. 10c), the temperature decreased at 1340 LST, and the variation in the temperature became small from 1350 LST. The long sunshine duration continued until 1600 LST. A SSW-ly wind developed after 1350 LST. The sea breeze passed over Gifu at around 1350 LST and covered most of the Noubi Plain. The "sea breeze front" was located between Gifu and Ibigawa.

At 1530 LST (Fig. 9d), the temperature at the foot of the mountains decreased slightly, and the gradient of the temperature over the Noubi Plain was small. Southerly or SSW-ly winds prevailed over the Noubi Plain and the foot of mountainous areas. A developed radar echo II appeared over the slope of the Ibuki Mountains.

At Ibigawa (Fig. 10b), the temperature decreased at 1500 LST, and the variation in the temperature became small. SSE-ly and southerly winds developed. Furthermore, the sunshine duration at Ibigawa became zero after

1450 LST. The sea breeze passed over Ibigawa. The sea breeze did not arrive at Tarumi on the slope of the Ibuki Mountains, because a southerly wind was not observed (Fig. 10a). The sea breeze front existed between Ibigawa and Tarumi. When the sea breeze front passed over Ibigawa, radar echo II occurred over the slope of the Ibuki Mountains. Radar echo II corresponds to cloud area II (Fig. 8b). The cumulonimbus cloud occurred and developed over the slope of the Ibuki Mountains when the sea breeze front arrived at the slope where the valley wind circulation developed.

Radar echo II with rainfall intensity over 64 mm h^{-1} remained stationary for about 2 hours from the occurrence (not shown). At Tarumi (Fig. 10a), a northerly wind with high temperature was observed between 1540 LST and 1640 LST. The warm airflow from the Ibuki Mountains side toward the cumulonimbus cloud existed when the cumulonimbus cloud was developing. A change of wind direction with low temperature was observed at 1650 LST and 1700 LST, coresponding to the outflow associated with the cumulonimbus cloud. The change in the wind direction with low temperature was also observed between 1550 LST and 1610 LST at Ibigawa (Fig. 10b). At Gifu (Fig. 10c), however, the SSW-ly and southerly wind with a slow decrease of temperature continued until 1700 LST.

4.3   Structure of the cumulonimbus cloud developed over the slope of the Ibuki Mountains

The structure of the cumulonimbus cloud observed by the Doppler radars over the slope of the Ibuki Mountains is described. In this subsection, a convective echo is defined by the radar reflectivity over 10 dBZ in a horizontal section of 4 km ASL, which almost corresponds to a cumulonimbus cloud. The cellular echo in the convective echo is defined by a strong and closed echo that had an intensity of 30 dBZ in a horizontal section of 4 km ASL. The cellular echo in the convective echo corresponds to a precipitating cell in the cumulonimbus cloud. We mainly focused on the period from 1506 LST to 1616 LST, when the cumulonimbus cloud was developing.

The cellular echoes in the present convective echo were organized along the direction of the
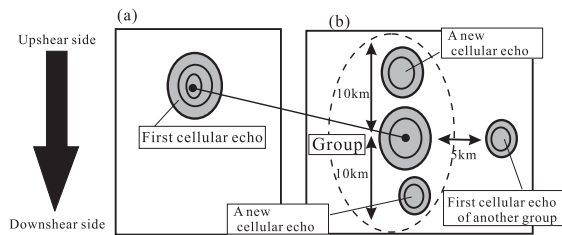
Fig. 11. Schematic representation of the method of the definition of a cellular echo group.

vertical wind shear of the environment. Figure 11 shows the schematic representation of the definition of a cellular echo group according to the following criteria.

When a cellular echo occurs without a cellular echo on the upshear and downshear sides of the environmental wind from the cellular echo, it is defined as a first cell (Fig. 11a). If another cellular echo occurs in the region within 10 km in both the upshear and downshear sides of the environment wind from the first cellular echo, the first cellular echo and its new cellular echo are regarded as part of the same cellular echo group. If a new cellular echo occurs in a region more than 5 km in the right-angled direction of the vertical wind shear in the environment from the group, it is regarded as the first cell of a new group (Fig. 11b).

The labels with letters of the alphabet indicate the cellular echo groups. The labels of numbers in the group indicate the order of appearance of cellular echoes. Number 1 is the "Primary Cell." Subsequent numbers are "Secondary Cells."

Figure 12a shows the topography of the slope of the Ibuki Mountains and the inner Noubi Plain. The direction of the gradient of the southward slope is from northwest to southeast. The direction of the gradient of the slope was nearly parallel to that of the vertical wind shear in the environment.

Figures 12b–12l show the time variation of the reflectivity of the echo observed by Doppler radars at 4 km ASL from 1506 LST to 1616 LST. Cellular echoes A1, A2, and B1 appeared at around 1506 LST (Fig. 12b). Cellular echoes A2 and B1 developed over 45 dBZ and cellular echo E1 appeared at 1520 LST (Fig. 12d). At

1527 LST (Fig. 12e), cellular echoes A3, B2, and E2 occurred on the upshear side of cellular echoes A2, B1, and E1, respectively.

At 1534 LST (Fig. 12f), cellular echoes B3 and B4 occurred near cellular echo B2. Cellular echoes C1 and D1 occurred between groups B and E. At 1541 LST (Fig. 12g), cellular echoes C3 and D2 occurred on the upshear side of cellular echoes C1 and D1, respectively. Furthermore, cellular echoes A4 and E3 occurred on the upshear side of cellular echoes A3 and E2, respectively. All cellular echoes developed to have reflectivity at 40 dBZ and above. A weak echo region began to extend to the downslope side, namely, the downshear side of cellular echoes at 1548 LST (Fig. 12h).

At 1555 LST (Fig. 12i), cellular echo C4 occurred on the upshear side of cellular echo C3. Cellular echo D3 occurred near cellular echo C3. Cellular echoes C3 and C4 merged and became a strong and large cellular echo, C3+C4, at 1602 LST (Fig. 12j). Cellular echo C3+C4 developed over 50 dBZ at 1616 LST (Fig. 12l). The reflectivity of cellular echo C3+C4 remained over 45 dBZ until 1705 LST (not shown). Cellular echo F1 occurred near cellular echo C3+C4 at 1602 LST (Fig. 12j). Cellular echo F2 developed on the upshear side of cellular echo F1 at 1609 LST (Fig. 12k).

Between weakening cellular echo E3 and developing cellular echo C3+C4, cellular echoes M and N occurred at 1555 LST and 1602 LST (Figs. 12i and 12j), respectively. They moved to the downslope side faster than the other cellular echoes. Because no cellular echo occurred on the upshear side of cellular echoes M and N, no group of cellular echoes was formed. Cellular echoes M and N will not be discussed in the present paper. Accordingly, the 6 groups of cellular echoes are noted as groups A, B, C, D, E, and F.

Figure 13a shows the occurrence points of cellular echoes. The occurrence points of cellular echoes aligned in the direction from northeast to southwest over the slope. Figures 13b–13g show the occurrence points, generating orders and tracks of the cellular echoes of the various groups. In groups A and D, Secondary cells occurred on the upshear side of the Primary Cell. In groups B and E, Secondary Cells occurred around the track of the Primary Cell. In groups C and F, some Secondary Cells oc-
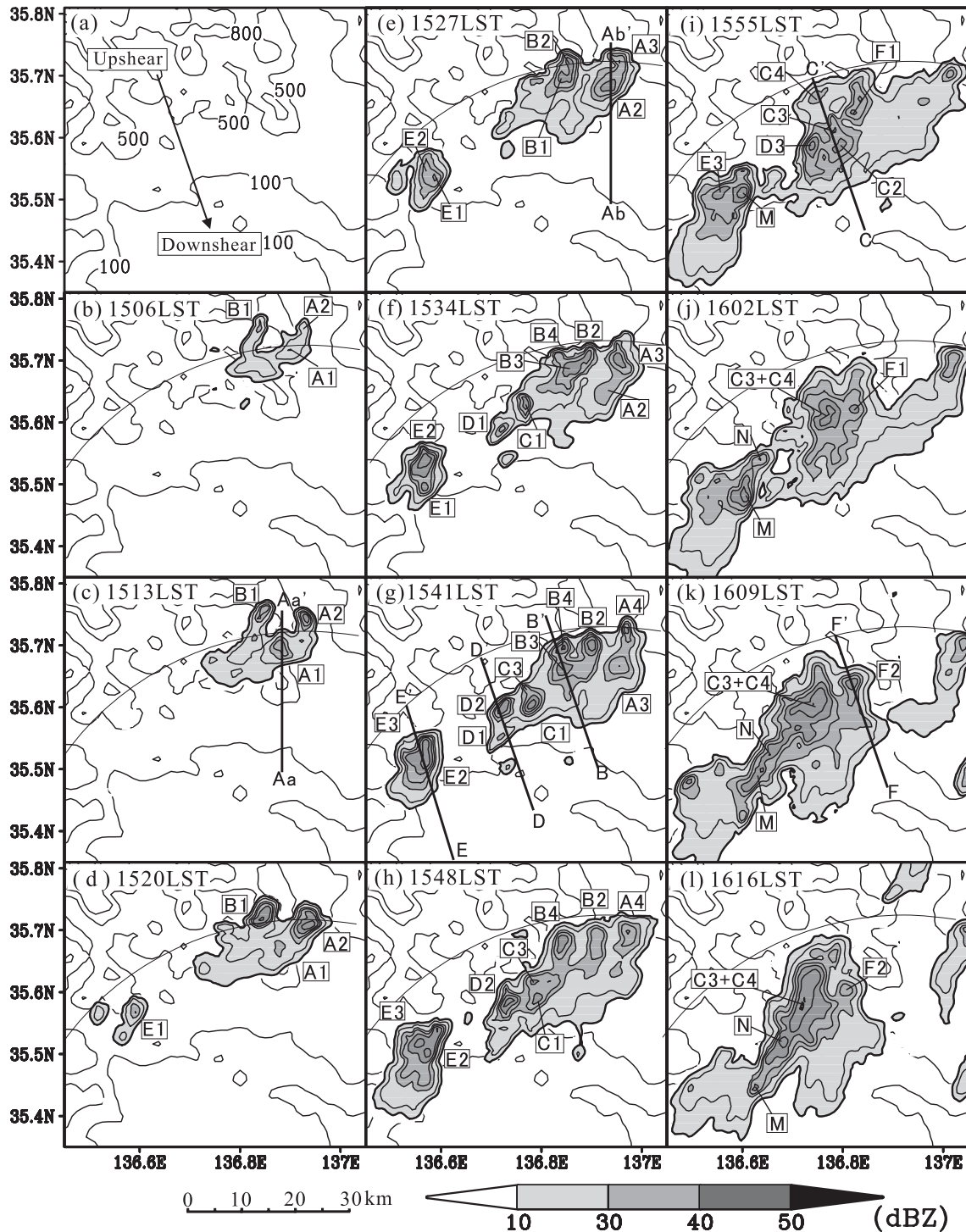
Fig. 12.   (a) Terrain of the slope of the Ibuki mountains. The arrow shows the direction of the vertical wind shear in environment. Time variation of a radar echo obtained by Doppler radars in (b)–(l). The shaded areas are the radar echoes. The contour intervals of the radar echoes are 10, 20, and every 5 dBZ from 30 dBZ. The contours of the topography are 100, 500, 800, and 1000 m. The arc lines in the figures are the range of the Doppler radar observation from Nagoya University.
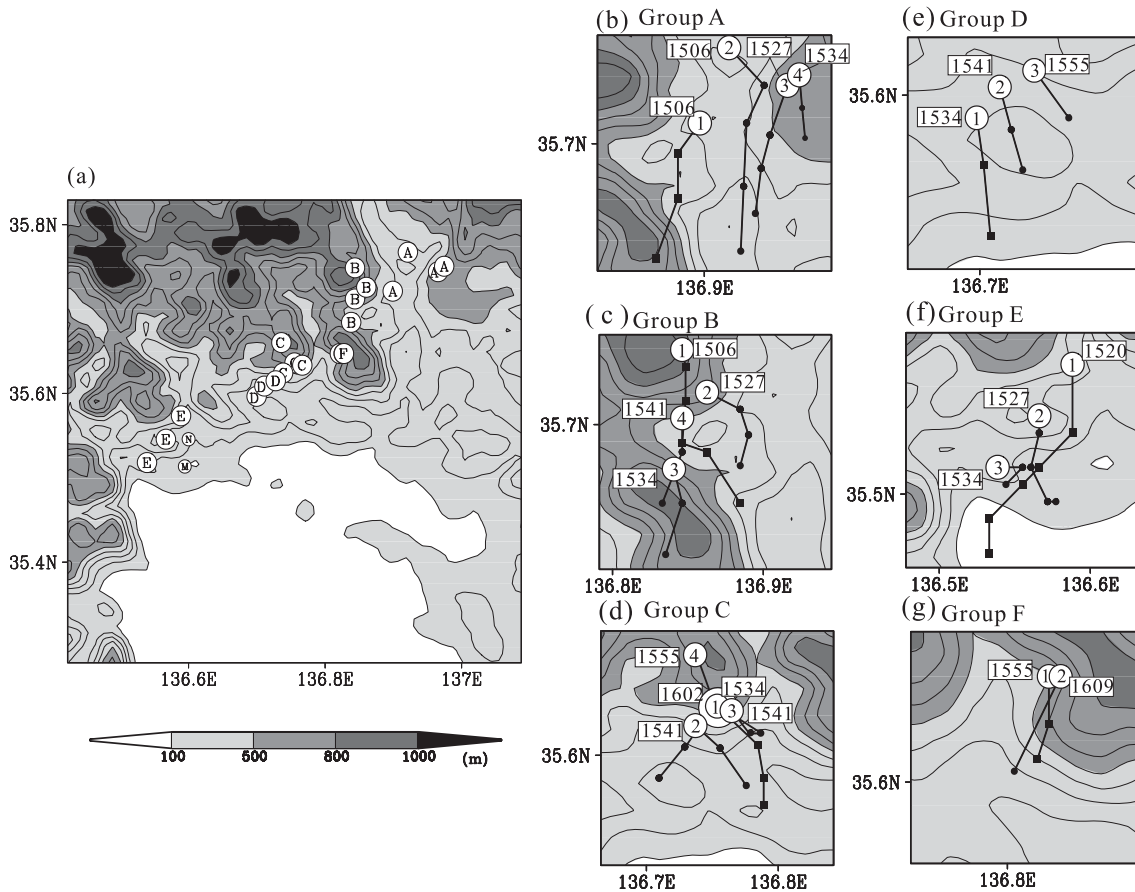
Fig. 13. (a) Occurrence points and track of cellular echoes. The open circles are the occurrence points of cellular echoes. A–F are cell groups. The shades indicate the topography. (b)–(g) Tracks of cellar echoes in each groups. The open circles are the occurrence points of cellular echoes. The order and time (LST) of cellular echoes in each group are indicated. The squares indicate the points of Primary cell at 7-minute intervals. The dots indicate the points of Secondary cells every 7 minutes. The shaded area indicates the topography.

curred at the same position in which the Primary Cell occurred. Cell C4 occurred on the upshear side of cell C1. The lifetimes of each cellular echo were between 20 and 30 minutes. The lifetimes of the cellular echo group, however, were about 50∼60 minutes, because new cellular echoes continuously occurred on the upshear side of pre-existing cellular echoes.

Figure 14 shows the vertical cross sections along the lines in Fig. 12 to show the structures of the "Primary Cell" and "Secondary Cells" in cellular echo groups, respectively. Primary Cells of each group, cells A1, B1, C1, D1, E1, and F1, were tilting toward the downslope side, namely the downshear side of the vertical wind shear of the environment. When Primary

cells weakened, they moved down the slope with tilting to the downshear side. In groups B, C, D, E, and F (Figs. 14b–14f), anvils extended to the downshear side at the upper layer.

Secondary Cells of each group occurred on the upshear side of the weakening Primary Cell. Secondary Cells developed almost uprightly. Secondary Cells developed more intensely than the Primary Cell in groups, respectively. In group A (Fig. 14a), cell A2 developed over 45 dBZ and cell A3 developed in the upshear side of cell A2. In group B (Fig. 14b), cell B3 fell on cell B1. Cell B3 developed over 45 dBZ and has a strong core at 8 km before 1541 LST (not shown). On the upshear
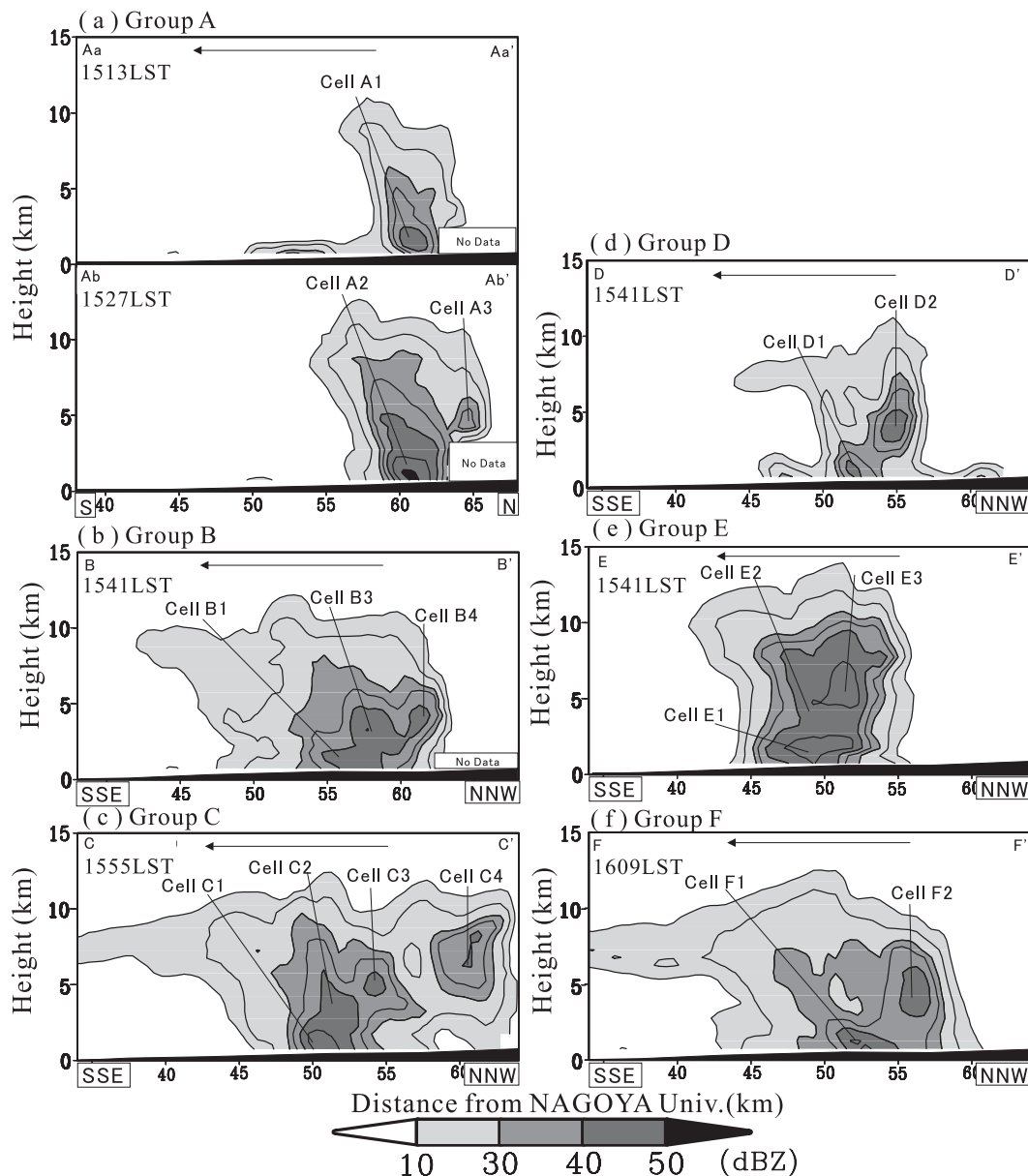
Fig. 14. Vertical cross session of the radar echo intensity of groups A, B, C, D, E, and F along the lines in Fig. 12. The contour intervals of the radar echo are 10, 20, and every 5 dBZ from 30 dBZ. The arrow is the direction of the vertical wind shear in environment.

side of cell B3, cell B4 developed uprightly. In group C (Fig. 14c), cells C2, C3, and C4 developed almost uprightly on the upshear side of cell C1. The cores of cells C2 and C3 were present at about 5 km ASL, while that of cell C4 was present at about 7 km ASL. In group D (Fig. 14d), cell D2 developed on the upshear side of cell D1. After that, cell D3 occurred on

the upshear side of cell D2 (not shown). In group E (Fig. 14e), cells E2 and E3 developed almost uprightly over cell E1. These cells had their strong cores at 7~8 km ASL. In group F (Fig. 14f), cell F2 also developed uprightly on the upshear side of weakening cell F1.

　The convective echo that developed over the slope of the Ibuki Mountains consisted of cellu-

lar echo groups. The groups consisted of the downshear tilting Primary Cell and upright Secondary Cells. Secondary Cells of each cellular echo group occurred on the upshear side of the Primary Cell of each group moving down the slope, which resulted in stationary of groups over the slope. The development of Secondary cells in each cellular echo group contributed to the development and long life of each cellular echo group. As a result, the cellular echo groups contributed to the long-term maintenance of the convective echo over the slope of the Ibuki Mountains.

To clarify the developing process and structure of a cellular echo group, the developing process and structure of group C are described in detail in the next subsection, because the structure and development of cellular echoes in group C were most clearly observed than those of the other groups by the dual Doppler radar observation.

4.4 Structure and evolution of the cellular echoes of group C

To clarify the motion of each cellular echo in group C, Fig. 15 shows the horizontal sections of the cellular echoes of group C at 1.5, 4.5 and 7 km ASL from 1534 LST to 1616 LST. Each cellular echo in group C developed in this period. The coordinates are rotated to 19° counterclockwise with the origin at Nagoya University (Fig. 15a). Following part of this subsection, the X- and Y-axes are defined in Fig. 15a. The position of the region of Fig. 15b is indicated by the thick rectangle in Fig. 15a. The Y and X are almost parallel and perpendicular, respectively, to the directions of the gradient of the southward slope of the Ibuki Mountains and the vertical wind shear of the environment.

Primary Cell C1 began to develop over the slope at 4.5 km ASL at 1534 LST. At 1541 LST, cell C1 developed over 45 dBZ with moving down the slope. The speed of cell C1 was fast. Cell C1 weakened from 1548 LST and a strong reflectivity region of cell C1 appeared at 1.5 km ASL only at 1555 LST. Cell C1 disappeared at 1602 LST.

On the upshear side of cell C1, Secondary Cell C2 occurred near cell C1 at 7 km ASL at 1541 LST. Cell C2 moved down the slope from 1548 LST. Cell C2 developed at 1555 LST and strong reflectivity appeared at 4.5 km ASL.

Cell C2 weakened from 1602 LST and the strong reflectivity region of cell C1 appeared at 1.5 km ASL only. Cell C2 disappeared at 1616 LST.

Secondary Cell C3 occurred at almost the same occurrence point of cell C1 at 4 km ASL at 1541 LST. Cell C3 developed and was stationary until 1555 LST. On the upshear side of the developed cell C3, Secondary cell C4 occurred. At 1602 LST, cells C3 and C4 merged and became cell C3+C4. Cell C3+C4 developed abruptly. Cell C3+C4 had a diameter of about 10 km at 7 km ASL at 1609 LST. Cell C3+C4 had maximum reflectivity over 50 dBZ at 1616 LST. The strong region of cell C3+C4 did not appear at 1.5 km ASL. Cell C3+C4 was stationary.

Figure 16 shows the vertical sections of the cellular echoes of group C along lines a-a′, b-b′ and c-c′ in Fig. 15b. Cell C1 occurred with downshear tilting at 1534 LST (Fig. 16a). Cell C1 developed with downshear tilting and moved down the slope at 1541 LST (Fig. 16b). The core of cell C1 developed over 45 dBZ at 4 km ASL. The anvil from cell C1 extended at the upper layer. The core of cell C1 fell to the slope at 1548 LST (Fig. 16c). Cell C1 weakened with downshear tilting and the anvil widely extended to the downshear side after 1555 LST (Fig. 16d).

Cell C2 occurred at 7∼8 km ASL on the upshear of cell C1 and the southwest side of cell C1 (Fig. 16e). Cell C2 moved to and developed over cell C1 (Fig. 16f), and appeared with slightly downshear tilting along line a-a′ (Fig. 16c). Cell C2 developed over 40 dBZ almost uprightly over cell C1 and had a height of over 10 km ASL (Figs. 16d and 16g). Cell C2 fell to the slope at 1602 LST (Fig. 16k) and weakened after 1609 LST (Fig. 16l).

Cell C3 occurred on the upshear side of cell C1 at 3 km ASL (Figs. 16b and 16h). Cell C3 developed almost uprightly and had a strong core at 5 km ASL at 1548 LST (Fig. 16c). In Fig. 16i, a low-reflectivity area existed under the core of cell C3. At 1555 LST, cell C3 developed more and the low reflectivity area were found below cell C3 (Figs. 16d and 16i).

Cell C4 developed almost uprightly on the upshear side of cell C3 at 1555 LST (Fig. 16d). Cell C4 had strong reflectivity between 5 and 10 km ASL.
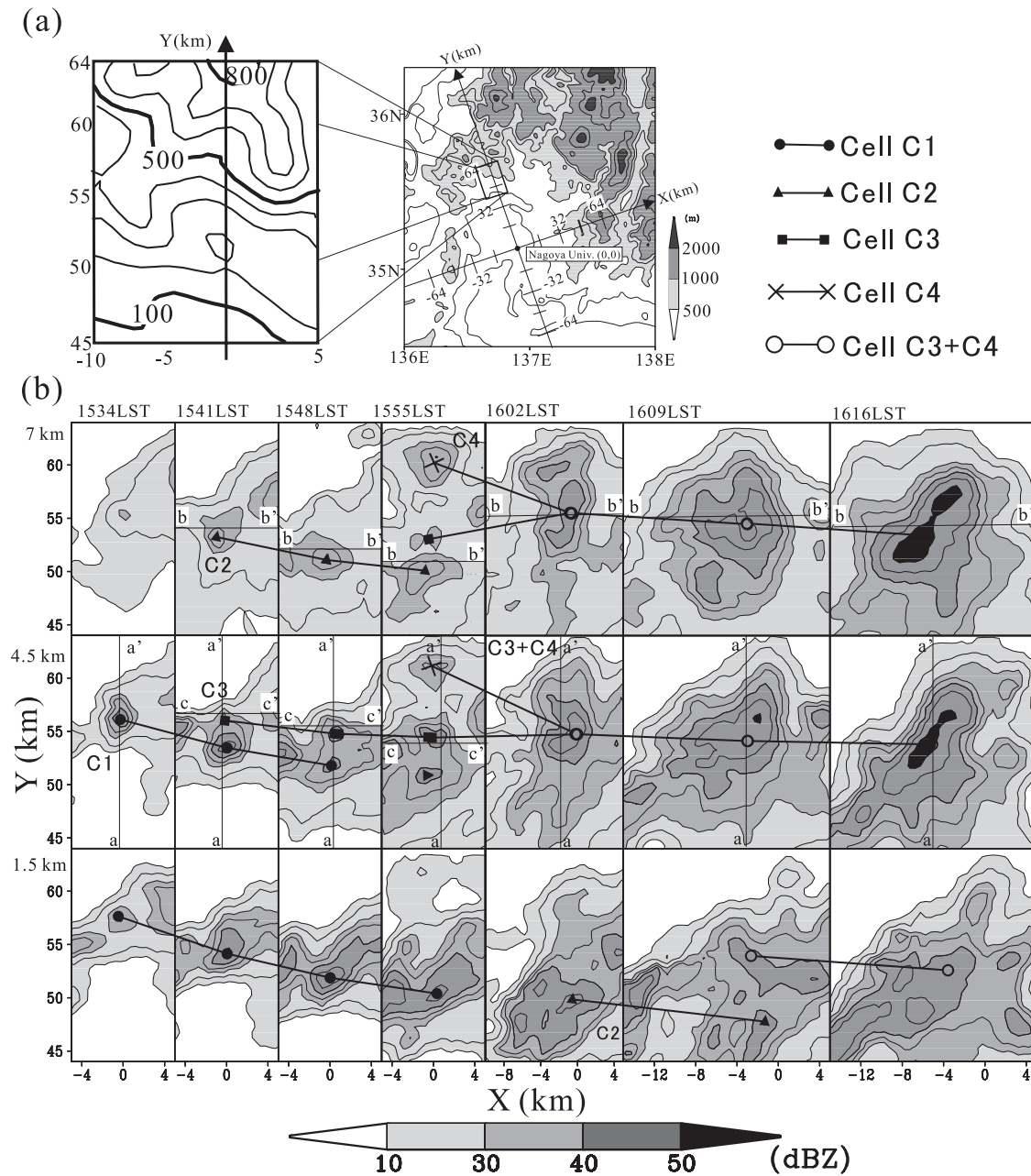
Fig. 15.   (a) Terrain map and X-Y grid rotated 19 degrees from the north. (b) Time variations of the cellular echoes of group C at 1.5, 4.5, and 7 km ASL. The shaded areas are the radar echoes. The contour intervals of the radar echoes are 10, 20, and every 5 dBZ from 30 dBZ.

Cell C3+C4 became a large upright cellular echo at 1602 LST (Figs. 16k and 16n). At 1609 LST, cell C3+C4 developed and had a horizontal scale over 10 km and an echo top about 15 km. At 1616 LST, cell C3+C4 developed more abruptly and had a core in excess of

50 dBZ reflectivity at 4∼9 km ASL and an echo top over 15 km ASL (Figs. 16l and 16o). In Fig. 16m, a low-reflectivity area existed under the core and a high-reflectivity area fell to the slope on the downshear side of the core. In Fig. 16p, a low-reflectivity area existed under
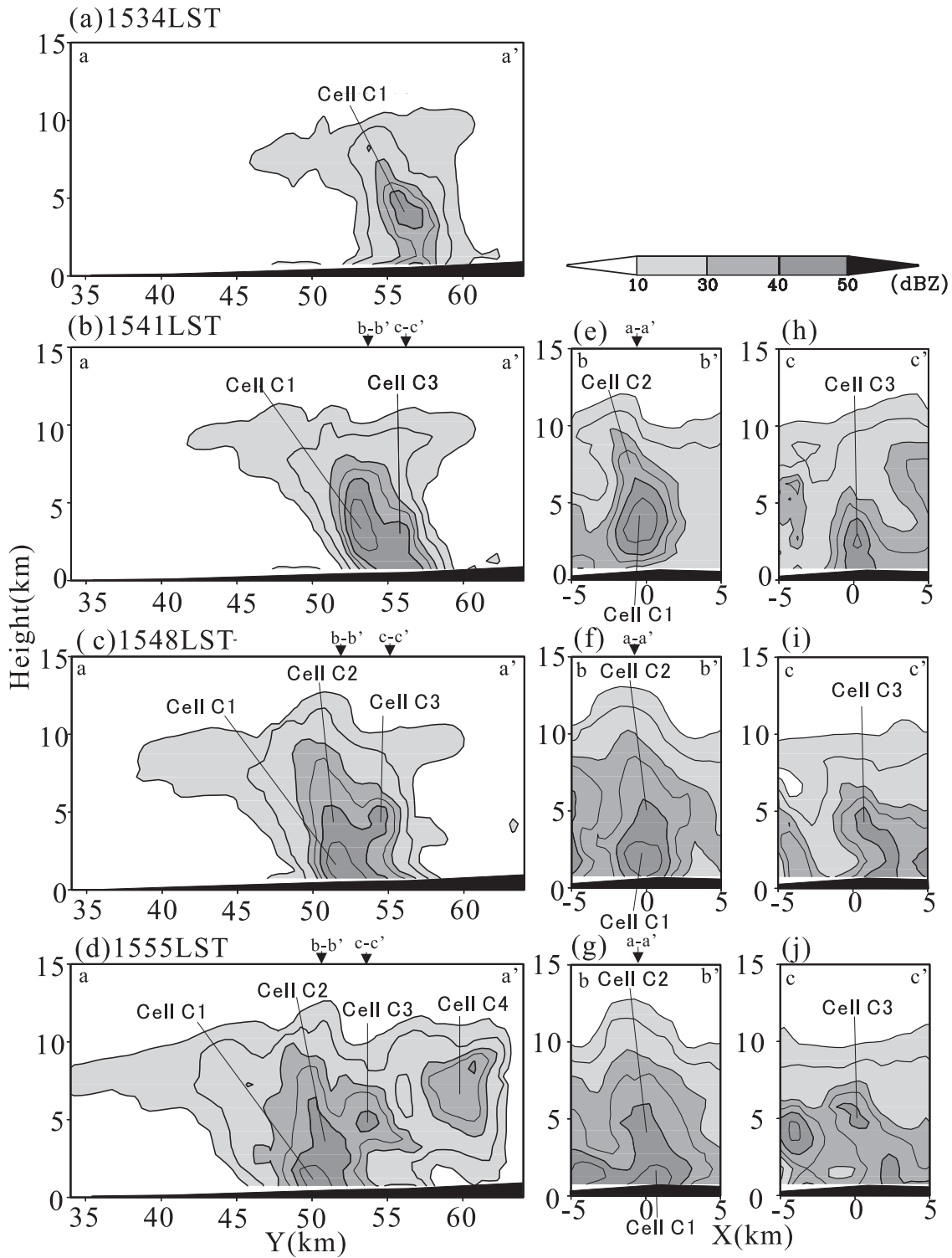
Fig. 16.   Vertical sections of cellular echoes of group C with the terrain along lines a-a′, b-b′ and c-c′ in Fig. 15 from 1534 LST to 1616 LST July 5, 2000. The contour intervals of the radar echo are 10, 20, and every 5 dBZ from 30 dBZ.
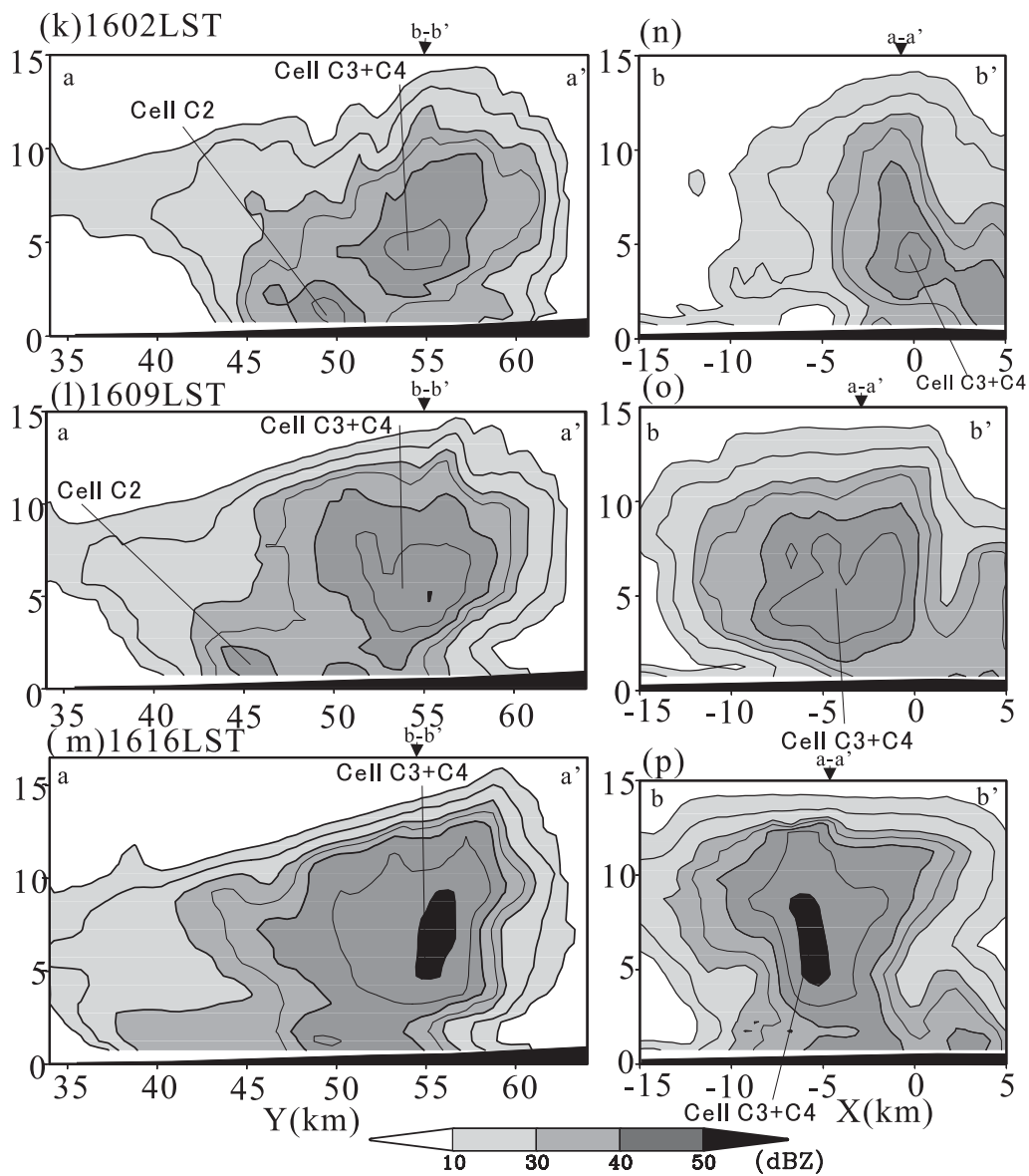
Fig. 16.   (continued)

Fig. 17.   Horizontal section at (a) 1.5 km ASL and (b) 2.5 km ASL of the ground-relative wind and
reflectivity of group C at 1555 LST July 5, 2000. The shaded areas indicate the reflectivity of the
radar echo. The contours of the reflectivity are 10, 20, and every 5 dBZ from 30 dBZ. The arrows in-
dicate the direction and speed of the ground-relative wind. The barb is the wind direction and speed
of wind at the Tarumi AMeDAS observation point at 1550 LST July 5, 2000. Vertical section of the
ground-relative velocity and reflectivity of the radar echoes along line a-a' in (c). Warm and cold col-
ors indicate the ground-relative velocity in parallel to the Y-axis in Fig. 15a toward the right side
and toward the left side in parallel to the vertical section, respectively. The white solid and dashed
contour indicate the ground-relative velocity in parallel to the X-axis in Fig. 15a every 4 m s^{-1} out of
and into the vertical section, respectively. The black contours of the radar echo are 10, 20, and every
5 dBZ from 30 dBZ. Vertical section of the horizontal divergence and reflectivity of cellular echoes
along line a-a' in (d). The warm and cold colors are the horizontal divergence and convergence,
respectively. The black contour lines of the radar echo are 10, 20, and every 5 dBZ from 30 dBZ.

the core and a high-reflectivity area fell to the slope on the right side of the core in this vertical section.

To examine Secondary Cells C3 and C4 which developed abruptly, the airflow in group C derived from the analysis of the dual Doppler radar observation at 1555 and 1602 LST is

shown in the following part of this section. Figures 17a and 17b show the reflectivity of group C and ground-relative wind derived from the analysis of the dual Doppler radar observations at 1.5 and 2.5 km ASL at 1555 LST. Figure 17c shows the reflectivity and ground-relative wind velocity in a vertical section along line a-a′ in

Fig. 17b. The vertical section along line a-a′ is parallel to the Y-axis in Fig. 15a and the same section in Fig. 16d. Figure 17d shows the reflectivity and horizontal divergence in a vertical section along line a-a′.

At 1555 LST, the outflow from the weakened cell C1 toward the upshear side of cell C1, namely toward the Ibuki Mountains, developed at 1.5 km ASL (Fig. 17a). The outflow from cell C2 toward the Ibuki Mountains developed at 2.5 km ASL (Fig. 17b). In the vertical section along line a-a′, large velocity toward the Ibuki Mountains side from cell C1 (Y = 49∼51 km and below 1.5 km ASL) developed (Fig. 17c). At the lower part of cell C2 (Y = 49∼53 km and at 1.5∼3 km ASL in Fig. 17c), large velocity toward the Ibuki Mountains side existed. These velocities corresponded to the outflow from cells C1 and C2, respectively. In Fig. 17d, a horizontal divergence in the low parts of cells C1 and C2 (Y = 47∼51 km and below 4 km ASL) and a horizontal convergence in the middle parts of cells C1 and C2 (Y = 49∼51 km and 4∼6 km ASL) developed, indicating that the outflows are associated with the downdrafts of cells C1 and C2.

In Fig. 17b, the inflow existed on the upshear side of cell C2 at 2.5 km ASL. Above the outflows from cells C1 and C2 (Y = 50∼62 km and 2∼5 km ASL in Fig. 17c), velocity from the Ibuki Mountains to group C developed. This velocity corresponds to the inflow at 2.5 km ASL in Fig. 17b. Thus, the inflow existed in the low parts of cells C3 and C4. A strong horizontal convergence developed in the low parts of cells C3 and C4, and in the middle part of cell C2 (Y = 50∼58 km and below 5 km ASL in Fig. 17d). A strong horizontal divergence existed in the upper parts of cells C2, C3, and C4, respectively. At Tarumi, a northerly wind was observed (Fig. 17a). The northerly wind at Tarumi blew between 1540 and 1640 LST when the cellular echoes in group C developed, with the temperature of 28∼29°C (Fig. 10a).

According to the results above, cell C1 was occupied by a downdraft. Cell C2 had a downdraft in the lower part and an updraft above the middle part. The outflows associated with the downdrafts from cells C1 and C2 lifted the inflow from the Ibuki Mountains on the upshear side of cells C1 and C2. As a result, cells C3 and C4 developed on the upshear side of cell C2.

Figure 18 shows the airflow in group C at 1602 LST when cell C3+C4 developed. Figures 18a and 18b show the reflectivity of group C, and ground-relative wind derived from an analysis of the dual Doppler radar observation at 1.5 and 4 km ASL at 1602 LST. Figures 18c and 18d show the reflectivity and ground-relative wind velocity in a vertical section along lines a-a′ and b-b′ in Fig. 18b.

The outflow toward the Ibuki Mountains side from weakened cells C2 developed below cell C3+C4 at 1.5 km ASL (Fig. 18a). In the vertical section along a-a′ (Fig. 18c), the outflow from cell C2, which weakened and fell to the slope, developed below 1.5 km ASL and at Y = 48∼55 km. The large velocity from cell C2 to cell C3+C4 in the middle part (Y = 47∼55 and at 1.5∼5 km ASL) is shown in Fig. 18c. At 4 km ASL (Fig. 18b), a NE-ly airflow toward group C rotated clockwise at group C. The positive velocity is the outflow from cell C2 at the lower level, and the rotated inflow to group C at the middle level.

A westerly airflow to cell C3+C4 existed at 4 km ASL (Fig. 18b). In the vertical section along b-b′ (Fig. 18d), the airflow developed at developing cell C3+C4 above the outflow from cell C2 and the rotated inflow. The westerly airflow to cell C3+C4 was the inflow from the Ibuki Mountains side lifted by the outflow from cell C2. The inflow formed a strong horizontal convergence with the rotated inflow in the middle part, which contributed to the abrupt development of cell C3+C4. The velocities at the upper part of cell C3+C4 (Fig. 18c) were smaller than those at 1555 LST (Fig. 17c). Cell C3+C4 developed almost uprightly with the weak wind in the upper part.

5. Discussion

5.1 Roles of the valley wind circulation and the sea breeze for the occurrence and evolution of the cumulonimbus cloud over the Ibuki Mountains

Using a two-dimensional numerical simulation of thermal circulation over a periodic valley, Kimura and Kuwagata (1995) described that heat is transported from the mountainous region to the valley region, and moisture is transported from the valley region to the mountainous region. Kuwagata et al. (1990) indi-

1602LST

Fig. 18.   Same as in Figs. 17a and 17b but for horizontal sections at (a) 1.5 km ASL and (b) 4 km ASL at 1602 LST. The barb is the wind direction and speed of wind at the Tarumi AMeDAS observation point at 1600 LST July 5, 2000. The same as in Fig. 17c but along (c) line a-a′ and (d) line d-d′ in Fig. 18b and at 1602 LST. The black and white arrowa in (c) and (d) are the directions of the positive and negative velocity in the vertical sections.

cated that the heating rate estimated from routine observational data was large in the inner plain and basin bottom because of the warm compensating subsidence of the upslope valley wind circulation. Kimura (1994) explained qualitatively that the decrease in the sunshine duration over mountainous regions corresponds to the increase of the precipitable water vapor over the mountainous regions. Before the cumulonimbus cloud occurred over the slope of the Ibuki Mountains, the temperature increased, a southerly wind developed at Ibigawa and Gifu (Figs. 10b and 10c), and sunshine duration was zero at Tarumi (Fig. 10a). Figures 9b and 9c show that the increase of the temperature in the inner Noubi Plain was larger than that along the coastal region of the Noubi Plain. We consider that the valley wind circulation developed between the Ibuki Mountains and the inner Noubi Plain, and resulted in the accumulation of heat in the inner Noubi Plain and water vapor on the upslope side of the Ibuki Mountains. The valley wind circulation created a favorable condition for the development of the cumulonimbus cloud over the Ibuki Mountains.

No cumulonimbus cloud, however, occurred over the Ibuki Mountains with the development of the valley wind circulation by 1500 LST. On the other hand, cumulonimbus clouds occurred over the northeast mountainous region which had a top of about 2 km ASL (Fig. 8b). As shown in Fig. 6, the convective mixed layer was developing at Hamamatsu at 0900 LST. The LFC at Hamamatsu at 0900 LST was about 3 km ASL (Section 4.1). Other triggers were necessary for the generation of the cumulonimbus cloud over the Ibuki Mountains, because of the high LFC, although the favorable condition for the development of the cumulonimbus cloud was created by the development of the valley wind circulation, and the convective mixed layer.

The sea breeze invaded the inner Noubi Plain (Figs. 9b–9d). No cumulonimbus cloud occurred over the Noubi Plain with the arrival of the sea breeze. Cumulonimbus clouds occurred over the slopes of the Ibuki Mountains and the Suzuka Mountains, with the arrival of the sea breeze (Figs. 9b and 9d). At Ibigawa, the sea breeze was observed from 1500 LST (Fig. 10b). The cumulonimbus cloud over the slope

of the Ibuki Mountains was observed by Doppler radar at 1506 LST (Fig. 12b). We consider that the updraft associated with the valley wind circulation over the slope of the Ibuki Mountains, was strengthened locally due to the low-level convergence along the sea breeze front. As a result, the cumulonimbus cloud occurred over the slope of the Ibuki Mountains.

A northerly wind, with high temperature, was observed at Tarumi for about 1 hour from 1540 LST, when the cumulonimbus cloud developed (Fig. 10a). The northerly wind was a downward wind over the slope of the Ibuki Mountains where the valley wind circulation developed. To develop the northerly wind over the slope, the pressure on the downslope side must drop below that on the upslope side. The northerly wind began to blow after the cumulonimbus cloud developed. It is considered that the northerly wind was caused by the pressure gradient associated with the local low-pressure area which resulted from the occurrence of the cumulonimbus cloud over the slope. The northerly wind developed in place of a valley wind over the slope, and contributed to the development of the cumulonimbus cloud as a warm and moist inflow from the Ibuki Mountains side.

5.2 *Structure and evolution of the cumulonimbus cloud developed over the slope of the Ibuki Mountains*

A Doppler radar observation indicated that the cumulonimbus cloud, which developed over the slope of the Ibuki Mountains, consisted of cell groups including Primary Cell and Secondary Cells. Secondary Cells of each cell group developed on the upshear side of each Primary Cell (Fig. 14).

Figure 19 shows the time variation of the ground-relative velocity in the vertical section of cell C1 at 1534 LST and 1541 LST. When cell C1 developed with tilting to the downshear side at 1534 LST, the slower ground-relative horizontal velocity ascended from the lower part of cell C1 along the core of cell C1, which resulted in the vertical gradient of the horizontal velocity along the cell C1 (Fig. 19a). It is considered that cell C1 was caused by the updraft associated with the valley wind circulation which was strengthened due to the low-level convergence along the sea breeze front,
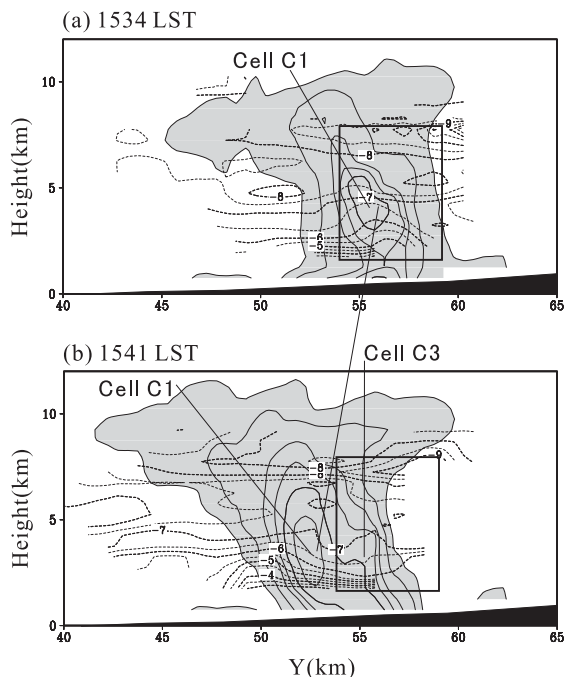
(a) 1534 LST

(b) 1541 LST

Y(km)

Fig. 19. Vertical section of group C along the lines a-a′ and b-b′ in Fig. 15 at 1534 LST and 1541 LST July 5, 2000. The thick contours indicate the ground-relative horizontal wind every 0.5 m s^{-1} in the vertical sections. The thin contours indicate 10, 20, and every 5 dBZ from 30 dBZ of radar reflectivity.

and the horizontal momentum at the lower layer, was transported to the middle layer.

At 1541 LST (Fig. 19b), cell C1 moved down the slope. The vertical gradient of the ground-relative horizontal velocity at cell C1 was large. The convection of cell C1 transported the horizontal momentum at the middle layer to the lower layer of the downshear side. While on the upshear side of cell C1, the vertical gradient of the ground-relative horizontal velocity became small, and cell C3 began to develop. It is considered that, on the upshear side, where vertical wind shear become weak, the outflow from cell C1 lifted the air which had small momentum at the lower layer, namely, the inflow from the Ibuki Mountains. As a result, almost upright Secondary Cells developed on the upshear side of cell C1.

When cells C3 and C4 developed at 1555 LST, the inflow in the lower layer lifted by the outflow from cell C1 formed a strong horizontal

convergence with the outflow associated to the downdraft of cell C2 at 2∼3 km ASL at 1555 LST (Figs. 17b–17d). Cells C3 and C4 developed by lifting the inflow by the outflow associated with the downdraft from cell C1, and the horizontal convergence in the middle layer by the outflow associated with the downdraft from cell C2. We consider that, from the structure in each cell group (Fig. 14), the inflow from the Ibuki Mountains side was lifted by the outflow from the Primary Cell in the lower layer. This resulted in the occurrence of Secondary Cells in each cell group.

When cell C3+C4 developed at 1602 LST, the inflow in the lower layer was lifted by the outflow from cell C1 and the NE-ly inflow to cell C3+C4 at 3∼5 km ASL (Figs. 18b–18d). When cell C3+C4 developed abruptly at 1616 LST, low reflectivity existed under the strong core of cell C3+C4 (Y = 55∼60 km in Fig. 16m and X = −10∼−5 km in Fig. 16p). The high-reflectivity area fell over the slope (Y = 49∼55 km in Fig. 16m and X = −5∼0 km in Fig. 16p). Furthermore, low reflectivity existed at X = −2∼0 km and 4∼6 km ASL in Fig. 16p. Geng et al. (1997) discussed that a convective cell in a thunderstorm developed above the merged outflows from the downdraft on the left frank of the convective cell, the downdraft on the rear flank of the convective cell, and the descending mid-level rear inflow. They mentioned that the mid-level rear inflow brought the dry environmental air into the thunderstorm, and initiated the downdraft on the rear flank of the convective cell by cooling of evaporation or sublimation. We consider that the downdraft of cell C2 was developed by the evaporative cooling associated with the dry air brought by the NE-ly inflow into group C at 3∼5 km ASL, and that the downdraft caused the outflow from cell C2. As a result, the lifting of the inflow from the Ibuki Mountains side by the outflow, and the horizontal convergence in the middle layer became very strong, and cell C3+C4 developed abruptly and uprightly. It is considered that the origin of the NE-ly inflow in the middle layer in the present study was a flow from the environment (Fig. 7), or a flow from the weakened cell groups A and B (Fig. 17b).

No developed cellular echo was observed on the downshear side of cell C1. An anvil extended to the downshear side of cell C1 from

cell C1 and to the lower layer of the down-shear side (Figs. 16c, 16d, 16k, 16l and 16m). A ground-relative velocity to the downshear side in the vertical section developed in the an-vil above 4 km ASL at 1555 LST (Fig. 17c). Horizontal convergence was observed in the an-vil at Y = 39~43 km and at 6 km ASL at 1555 LST (Fig. 17d). Brown (1979) found in the nu-merical study that evaporation of anvil rain can induce a mesoscale downdraft beneath the anvil. Stensrud et al. (1991) discussed the maintenance and strengthening of the meso-scale downdraft in the anvil associated with sublimation, evaporation, and melting in the numerical study. Grady and Verlinde (1997) showed the structure of a squall line with a leading anvil and discussed the suppression associated with the leading anvil of convection on the downshear side of the squall line. It is considered that the occurrence of a new cell on the downshear side of cell C1 was suppressed by the mesoscale downward motion associated with the anvil.

The sea breeze developed on the downshear side (Fig. 9). At Gifu (Fig. 10c), the sea breeze was observed from 1350 LST and the temper-ature decreased. The sunshine duration re-mained long until 1500 LST. After 1500 LST, the sunshine duration decreased, which was a result of the anvil extending from the cumulo-nimbus cloud over the slope of the Ibuki Moun-tains. In addition to the suppression of convec-tion below the anvil, we consider that it is difficult for a new cellular echo on the down-shear side to be generated by lifting the sea breeze by the outflow from cell C1, because the sea breeze is a cold advection.

The structure and evolution of the cumulo-nimbus cloud in the present study are different from those in previous studies of cumulonim-bus clouds developed over mountains. Cara-cena et al. (1979) and Yoshizaki and Ogura (1988) explained, when the wind toward the slope was strong in the lower level and weak in the upper level, new convective cells oc-curred at the foot of the slope, and moved up the slope one after another because of the sta-tionary inflow of water vapor in the lower level. Cotton et al. (1983) and Tripoli and Cotton (1989) indicated that cumulonimbus clouds of the mesoscale convective complex occurred around the top of the slope and propagated to-
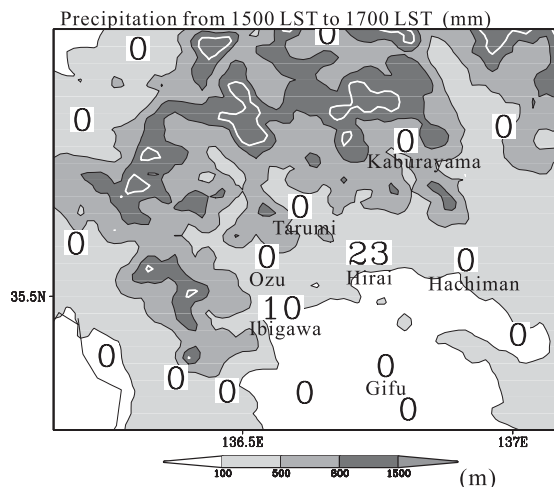

Fig. 20.   Precipitation from 1500 LST to 1700 LST July 5, 2000 at each AMeDAS observation point over the slope of the Ibuki Mountains. The shaded areas are the topography. The black contours at 100, 500 and 800 m ASL. The white contours at 1000 m ASL.

ward the downslope side, namely the down-shear side in the vertical environmental wind shear. The difference between the present study and previous studies is the occurrence of Secondary Cells on the upslope side of the mountains, namely the upshear side of the Primary Cell, and the lack of occurrence of a new cumulonimbus cloud on the downslope side of the mountains, namely the downshear side of the Primary Cell.

The successive development of the cell groups contributed to the development and mainte-nance of a cumulonimbus cloud over the slope of the mountains for a long time. The cumulo-nimbus cloud then caused heavy rainfall over the mountainous region. Figure 20 shows the precipitation from 1500 LST and 1700 LST over and around the slope of the Ibuki Moun-tains. In the present study local heavy rainfall at the surface, associated with the developed cumulonimbus cloud was observed over and around the slope of the Ibuki Mountains. This rainfall was 23 mm at Hirai and 10 mm at Ibi-gawa.

6.   Summary

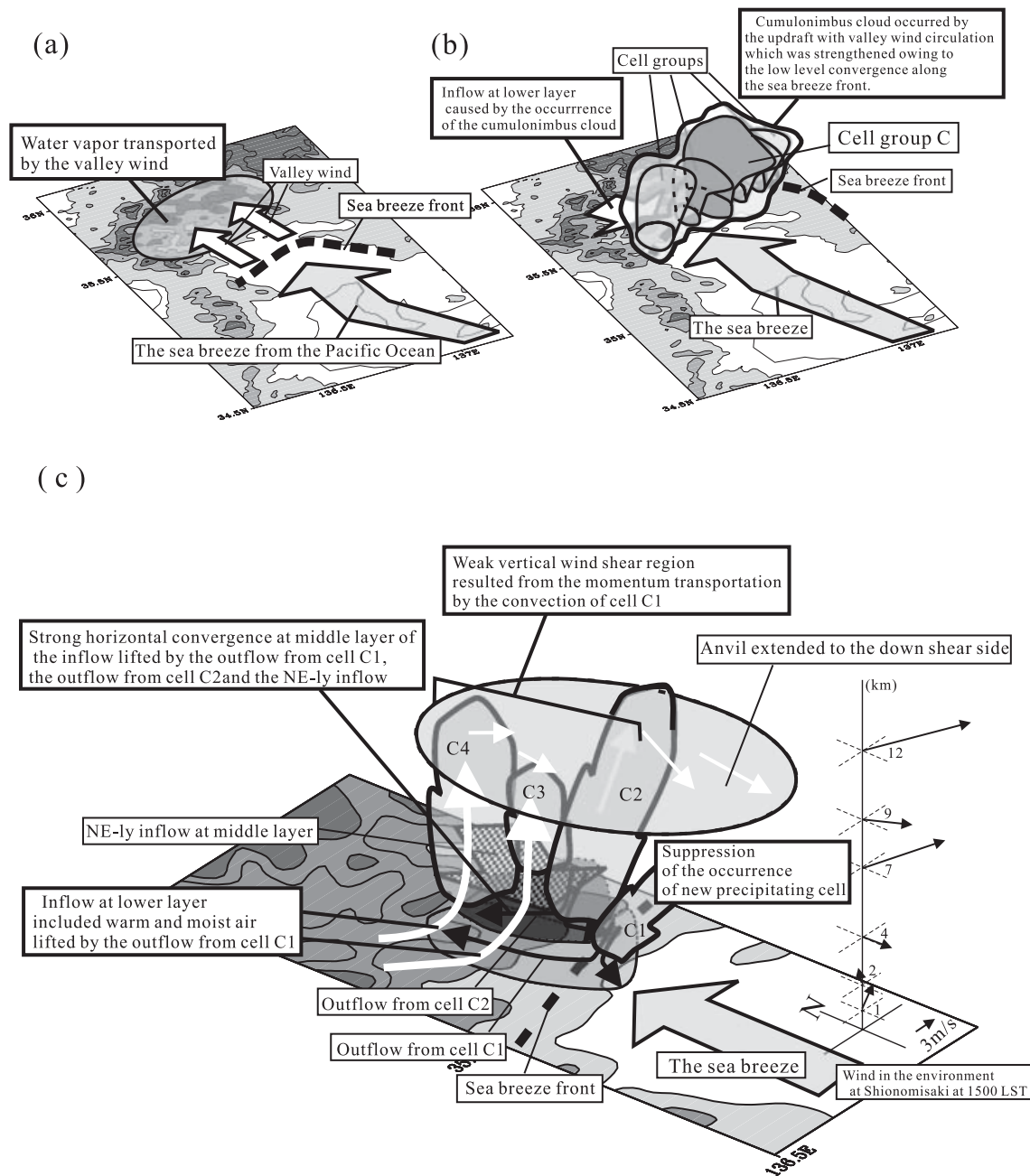The cumulonimbus cloud that developed over

Fig. 21. Schematic figures of (a) the valley wind and sea breeze before the cumulonimbus cloud occurred over the slope of the Ibuki Mountains on July 5, 2000, (b) the structure of the cumulonimbus cloud developed over the slope of the Ibuki Mountains, and (c) the structure of cell group C in the cumulonimbus cloud developed over the slope of the Ibuki Mountains.

the slope of the Ibuki Mountains in summer was studied in detail, with the use of data of Doppler radar observations. From the results of this analysis, we discussed the structure and evolution of the cumulonimbus cloud as follows

(Fig. 21).

Before the occurrence of the cumulonimbus cloud, a valley wind developed over the slope of the Ibuki Mountains, and the sea breeze from the Pacific Ocean blew over the Noubi Plain

(Fig. 21a). We consider that the valley wind circulation resulted in a favorable field for the occurrence of a cumulonimbus cloud. When the sea breeze front arrived at the slope of the Ibuki Mountains where the valley wind circulation developed, the cumulonimbus cloud occurred (Fig. 21b). We consider that the cumulonimbus cloud was caused by the updraft associated with the valley wind circulation over the slope, which was strengthened locally due to the low-level convergence along the sea breeze front. The occurrence of the cumulonimbus cloud caused the inflow from the Ibuki Mountains side to the cumulonimbus cloud. This inflow contributed to the development of the cumulonimbus cloud.

The cumulonimbus cloud consisted of cell groups which include Primary Cell and Secondary Cells. We focused on group C, in which the cells developed more. Over the slope, which was nearly parallel to the direction of the vertical wind shear of the environment, Primary Cell C1 was tilting to the downshear side and Secondary Cells C2, C3, and C4 were almost upright (Fig. 21c). Secondary cells occurred by the inflow from the Ibuki Mountains side lifted by the outflow from cell C1. Cell C3+C4, which merged cells C3 and C4, developed abruptly because of the strengthening of the horizontal convergence in the middle layer by the NE-ly inflow toward cell C3+C4. A weak vertical wind shear region was formed on the upshear side of cell C1, because the convection of cell C1 transported the horizontal momentum in the middle layer. Therefore, we consider that Secondary Cells develop almost uprightly on the upshear side of cells C2, C3, and C4. It is considered that the anvil extended to the downshear side suppressed the occurrence of a new cellular echo on the downshear side.

We clarified one of the structure and evolution of a cumulonimbus cloud occurred in a field which thermally induced local circulations developed. The arrival of a sea breeze at the slope with a valley wind circulation triggered the occurrence of a cumulonimbus cloud. The outflow from the Primary Cell lifted the moist air over the slope of the Ibuki Mountains accumulated by the valley wind. Secondary Cells developed almost uprightly on the upshear side of the Primary Cell. As a result, the cumulonimbus cloud was almost stationary,

and brought heavy rainfall to the local mountainous region. The cumulonimbus cloud played one part in the water circulation process associated with thermally induced local circulations.

References

Atkins, N.T. and R.M. Wakimoto, 1995: Observations of the sea-breeze front during CaPE. Part II: Dual-Doppler and aircraft analysis. *Mon. Wea. Rev.*, **123**, 944–969.

Atkinson, B.W., 1981: *Meso-scale Atmospheric Circulations*. Academic Press, 495pp.

Brown, J.M., 1979: Mesoscale unsaturated downdrafts driven by rainfall evaporation: a numerical study. *J. Atmos. Sci.*, **36**, 313–338.

Caracena, F.C., R.A. Maddox, L.R. Hoxit, and C.F. Chappell, 1979: Mesoanalysis of the Big Thompson Storm. *Mon. Wea. Rev.*, **107**, 1–17.

Chuda, T. and H. Niino, 2005: Climatology of environmental parameters for mesoscale convections in Japan. *J. Meteor. Soc. Japan*, **83**, 391–408.

Cotton, R.W., R.L. George, P.J. Wetzel, and R.L. Mcanelly, 1983: A long-lived mesoscale convective complex. Part I: The mountain-generated component. *Mon. Wea. Rev.*, **111**, 1893–1918.

Cressman, G.P., 1959: An operational objective anal-

ysis system. *Mon. Wea. Rev.*, **87**, 367–374.

Dailey, P.S. and R.G. Fovell, 1999: Numerical simulation of the interaction between the sea-breeze front and horizontal convective rolls. Part I: Offshore ambient flow. *Mon. Wea. Rev.*, **127**, 858–878.

Fujibe, F., 1988: Diurnal variations of precipitation and thunderstorm frequency in Japan in warm season. *Pap. Meteor. Geophys*, **39**, 79–94.

Gal-Chen, T., 1982: Errors in fixed and moving frame of reference: Doppler radar analysis. *J. Atmos. Sci.*, **39**, 2279–2300.

Geng, B., Y. Fujiyoshi, and T. Takeda, 1997: Evolution of a multicell thunderstorm in association with mid-level rear inflow enhanced by a mid-level vortex in an adjacent thunderstorm. *J. Meteor. Soc. Japan*, **75**, 619–637.

Grady, R.L. and J. Verlinde, 1997: Triple-Doppler analysis of a discretely propagating, long-lived high plains squall line. *J. Atmos. Sci.*, **54**, 2729–2748.

Iwasaki, H., 2004: Diurnal variation of precipitable water and convective activity with dual maxima in summer season around Mt. Tanigawa in the Northern Kanto District, Japan. *J. Meteor. Soc. Japan*, **82**, 805–816.

——— and T. Miki, 2001: Observational study on the diurnal variation in precipitable water associated with the thermally induced local circulation over the "semi-basin" around Maebashi using GPS data. *J. Meteor. Soc. Japan*, **79**, 1077–1091.

——— and Y. Ohbayashi, 1998: Some characteristic of hailstorms over Gunma Prefecture. *Tenki*, **45**, 695–705 (in Japanese).

Kimura, F., R. Tanigawa, and M. Yoshizaki, 1997: Diurnal variation of precipitable water in clear days over the Northern Mountains in Kanto Plain. *Tenki*, **44**, 799–807 (in Japanese).

———, 1994: Horizontal transport of moisture by local circulation—Duration of sunshine depending on the topography in cloudless day—. *Tenki*, **41**, 313–320 (in Japanese).

——— and T. Kuwagata, 1995: Horizontal heat fluxes over complex terrain computed using a simple mixed-layer model and a numerical model. *J. Appl. Meteor.*, **34**, 549–558.

Kingsmill, D.E., 1995: Convection initiation associated with a sea-breeze front, a gust front, and there collision. *Mon. Wea. Rev.*, **123**, 2913–2933.

Kondo, H., 1990a: A Numerical experiment of the "extended sea breeze" over the Kanto Plain. *J. Meteor. Soc. Japan*, **68**, 419–434.

———, 1990b: A Numerical experiment on the interaction between sea breeze and valley wind to generate the so-called "extended sea breeze". *J. Meteor. Soc. Japan*, **68**, 435–446.

Kurita, H., H. Ueda, and S. Mitsumoto, 1988: Three-dimensional meteorological structure of long-range transport of air pollution under light gradient wind. *Tenki*, **35**, 23–35 (in Japanese).

Kuwagata, T., M. Sumioka, N. Masuko, and J. Kondo, 1990: The daytime PBL heating process over complex terrain in Central Japan under fair and calm weather conditions. Part I: Meso-scale circulation and the PBL heating rate. *J. Meteor. Soc. Japan*, **68**, 625–638.

———, 1997: An analysis of summer rain showers Central Japan and its relation with the thermally induced circulation. *J. Meteor. Soc. Japan*, **75**, 513–527.

——— and F. Kimura, 1995: Daytime boundary layer evolution in a deep valley. Part I: Observations in the Ina Valley. *J. Appl. Meteor.*, **34**, 1082–1091.

——— and ———, 1997: Daytime boundary layer evolution in a deep valley. Part II: Numerical simulation of the cross-valley circulation. *J. Appl. Meteor.*, **36**, 883–895.

Mori, H., H. Ogawa, and T. Kitada, 1994: Characteristics of land and sea breeze in the Noubi plain, and the conditions of occurrence of the "extended sea breeze". *Tenki*, **41**, 379–385 (in Japanese).

Nicholls, M.E., R.A. Pielke, and W.R. Cotton, 1991: A two-dimensional numerical investigation of the interaction between sea breezes and deep convection over the Florida peninsula. *Mon. Wea. Rev.*, **119**, 298–323.

Owada, M., 1994: *Atmospheric Environment of the Ise-Bay and its Surrounding Area*. Nagoya University Press, 219 pp (in Japanese).

Pielke, R.A., 1974: A three-dimensional numerical model of the sea breezes over South Florida. *Mon. Wea. Rev.*, **102**, 115–139.

———, 1991: The predictability of sea-breeze generated thunderstorms. *Atmosfera*, **4**, 65–78.

Saitoh, T. and F. Kimura, 1998: Diurnal variation of convective precipitation in Chubu—Kanto area in the summer. *Tenki*, **45**, 541–549 (in Japanese).

Sasaki, T. and F. Kimura, 2001: Diurnal variation of water vapor content over the Kanoto area during clear summer days observed through GPS precipitable water. *Tenki*, **48**, 65–74 (in Japanese).

Simpson, J.N., N.E. Westcott, R.J. Clerman, and R.A. Pielke, 1980: On cumulus mergers. *Arch. Meteor. Geophys. Bioklimatol*, **29**, 1–40.

Stensrud, D.J., R.A. Maddox, and C.L. Ziegler, 1991: A sublimation-initiated mesoscale downdraft

and its relationto the wind field blew a precipitating anvil cloud. *Mon. Wea. Rev.*, **119**, 2124–2139.

Tripoli, J.G. and W.R. Cotton, 1989: Numerical study of an observed organic mesoscale convective system. Part I: Simulated genesis and comparison with observations. *Mon. Wea. Rev.*, **117**, 273–304.

Wakimoto, R.M. and N.T. Atkins, 1994: Observations of the sea-breeze front during CaPE. Part I: Single-Doppler, satellite, and cloud pho-

togrammetry analysis. *Mon. Wea. Rev.*, **122**, 1092–1114.

Wilson, J.W. and D.L. Megenhardt, 1997: Thunderstorm initiation, organization, and lifetime associated with Florida boundary layer convergence lines. *Mon. Wea. Rev.*, **125**, 1507–1525.

Yoshizaki, M. and Y. Ogura, 1988: Two- and Three-dimensional modeling of the Big Thompson Storm. *J. Atmos. Sci.*, **45**, 3700–3722.